The solutions and tunneling properties for a linear potential and an inverted harmonic oscillator in an infinite well

Pro gradu -tutkielma
Turun yliopisto
Fysiikan ja tähtitieteen laitos
Teoreettinen fysiikka
2015
Tuomas Riihimäki
Tarkastajat:
prof. Kalle-Antti Suominen
dosentti Tom Kuusela

TURUN YLIOPISTO
Fysiikan ja tähtitieteen laitos
RIIHIMÄKI, TUOMAS: Lineaarisen potentiaalin ja käännetyn harmonisen oskilaattorin ratkaisuja ja tunnelointiominaisuuksia äärettömän syvässä laatikossa
Pro gradu-tutkielma 79 s., 4 liitesivua
Teoreettinen fysiikka
Lokakuu 2015

Tässä työssä tarkastellaan kahta erilaista 1-ulotteista kvanttimekaanista systeemiä. Näiden systeemien potentiaalit ovat lineaarinen potentiaali äärettömän syvässä kaivossa ja käännetty harmoninen oskillaattori äärettömän syvässä kaivossa. Näille molemmille tapauksille etsitään energian ominaisarvot ja -funktiot ratkaisemalla systeemin Schrödingerin yhtälö. Ratkaisut saadaan käyttämällä reunaehtoja ja hyödyntämällä numeerisia menetelmiä. Motivaatio näiden ratkaisujen tarpeelle tulee kokeellisesta taustasta.

Lineaarisen potentiaalin tapauksessa reunaehtoja on kaksi. Ensimmäinen on niin sanottu normaaliehto, jossa aaltofunktio on nolla laatikon reunoilla. Toisena on derivaattaehto, jossa taas vuorostaan aaltofunktion derivaatta on nolla laatikon reunoilla. Aaltofunktion ratkaisut ovat Airyn funktioita. Käännetyn harmonisen oskillaattorin tapauksessa tarkastellaan normaalia reunaehtoa ja ratkaisut ovat vuorostaan parabolisia sylinterifunktioita. Molempien yhteydessä tehdään vertailua hiukkanen laatikossa -ratkaisuun. Tulosten yhteydessä esitellään myös kuvia ja taulukoita, joista selviää sekä energian ominaisfunktioiden ulkonäkö että yhteydet hiukkanen laatikossa -problematiikkaan. Kuvien ja laskujen kanssa on käytetty matemaattisia ohjelmistoja. Lineaarista potentiaalia verrataan myös tapaukseen, jossa ääretön reuna on vain vasemmalla puolella. Tästä tapauksesta esitellään myös graafisia todisteita näiden systeemien yhtäläisyyksistä ja eroavaisuuksista.

Näiden lisäksi käännetyn harmonisen oskillaattorin tapauksessa perehdytään vielä tunnelointiproblematiikkaan. Sen yhteydessä käydään läpi hieman kvanttitunneloinnin historiaa, sen kehittäjiä ja lopuksi esitellään Feynmannin polkuintegraaliteoria. Tämän avulla saadaan instantoniratkaisut, joita voidaan käyttää tunnelointiominaisuuksien tarkastelussa. Tunnelointitapausta vertaillaan kaksoiskuoppapotentiaaliin, joka on systeeminä hyvin vastaavanlainen kuin tarkasteltava potentiaali. Ratkaisut saadaan myös samanlaisilla menetelmillä, joten vertailu on helppoa.

Kaiken kaikkiaan työssä myös pohditaan ja käydään läpi myös kvanttimekaniikan kehitysvaiheita ja erilaisia tapoja tulkita kvanttiteoriaa. Tämän ohessa myös esitellään erikseen ratkaisuissa tarvittavia erikoisfunktioita, niiden ominaisuuksia ja erilaisia yhteyksiä muihin erikoisfunktioihin. On olennaista huomata, että on mahdollista käyttää erilaisia matemaattisia formalismeja halutun lopputuloksen saamiseksi. Kvanttimekaniikka on rakentunut noin sadan vuoden aikana teoriaksi, jolle löytyy monenlaisia lähestymistapoja. Erilaiset tavat mahdollistavat eri asioiden tutkimista.

Asiasanat: Schrödingerin yhtälö, kvanttitunnelointi, instantoni, Feynmanin polkuintegraali, erikoisfunktiot

TURKU UNIVERSITY
Department of Physics and Astronomy
RIIHIMÄKI, TUOMAS: The solutions and tunneling properties for a linear potential and an inverted harmonic oscillator in an infinite well
Pro gradu-thesis 79 p., 4 appendix p.
Theoretical Physics
October 2015

In this work we look at two different 1-dimensional quantum systems. The potentials for these systems are a linear potential in an infinite well and an inverted harmonic oscillator in an infinite well. We will solve the Schrödinger equation for both of these systems and get the energy eigenvalues and eigenfunctions. The solutions are obtained by using the boundary conditions and numerical methods. The motivation for our study comes from experimental background.

For the linear potential we have two different boundary conditions. The first one is the so called normal boundary condition in which the wave function goes to zero on the edge of the well. The second condition is called derivative boundary condition in which the derivative of the wave function goes to zero on the edge of the well. The actual solutions are Airy functions. In the case of the inverted oscillator the solutions are parabolic cylinder functions and they are solved only using the normal boundary condition. Both of the potentials are compared with the particle in a box solutions. We will also present figures and tables from which we can see how the solutions look like. The similarities and differences with the particle in a box solution are also shown visually. The figures and calculations are done using mathematical software. We will also compare the linear potential to a case where the infinite wall is only on the left side. For this case we will also show graphical information of the different properties.

With the inverted harmonic oscillator we will take a closer look at the quantum mechanical tunneling. We present some of the history of the quantum tunneling theory, its developers and finally we show the Feynman path integral theory. This theory enables us to get the instanton solutions. The instanton solutions are a way to look at the tunneling properties of the quantum system. The results are compared with the solutions of the double-well potential which is very similar to our case as a quantum system. The solutions are obtained using the same methods which makes the comparison relatively easy.

All in all we consider and go through some of the stages of the quantum theory. We also look at the different ways to interpret the theory. We also present the special functions that are needed in our solutions, and look at the properties and different relations to other special functions. It is essential to notice that it is possible to use different mathematical formalisms to get the desired result. The quantum theory has been built for over one hundred years and it has different approaches. Different aspects make it possible to look at different things.

Key words: Schrödinger equation, quantum tunneling, instanton, Feynman path integral, special functions

Contents

1 Introduction

Quantum mechanics became a very relevant field of study in the beginning of the 20th century. The quantum theory is very powerful and has many intriguing problems. The phenomena are mostly not seen in the macroscopic scale and therefore they might seem a bit hard to comprehend. The logic of the world observed by our eyes does not work in the same way when we go into the Planck length scale. The Planck length is defined by the Planck constant h, the speed of light c and the gravitational constant G. These are all called fundamental physical constants that are the same everywhere in our universe. The Planck length itself is denoted by L_P and defined by

$$L_P = \sqrt{\frac{\hbar G}{c^3}} \approx 1,616 \times 10^{-35} m. \tag{1}$$

The reduced Planck constant is denoted by $\hbar$ and it is related to the Planck constant h by a simple equation

$$\hbar = \frac{h}{2\pi}. \tag{2}$$

Max Planck was a famous German physist who actually planted the seeds for the quantum theory, and can be thought of as a father for the quantum theory. He also played a key role in formulating the theory of statistical mechanics. [1]

The name of the quantum theory comes from the Latin word 'quanta' which follows from the observation that some physical quantities, e.g. energy, can change only in discrete amounts. Two basic tools in the mathematical formalism of the quantum theory are the wave function, which contains information about the probability amplitude of particle's physical properties such as position and momentum, and the Schrödinger equation, which can be used to formulate the time evolution of a quantum state and also to calculate the energy eigenvalues and eigenfunctions. This means that the wave function can be solved using the Schrödinger equation, which is usually written as [2]

$$-\frac{\hbar^2}{2m}\nabla^2\Psi + V\Psi = i\hbar\frac{\partial\Psi}{\partial t}, \tag{3}$$

where $\hbar$ is the reduced Planck constant, m is the particle mass, V is the potential, and Ψ is the wave function for which the whole operator equation operates. The

right hand side can also be written as [2]

$$i\hbar\frac{\partial\Psi}{\partial t} = E\Psi, \tag{4}$$

where E stands for the energy of the system. Even though the quantum theory contains very much abstract mathematics it also has lots of different ways to interpret how the results have gotten their form. What actually happens in the middle where the measurement results and mathematics tell us nothing?

The mathematical formalism of quantum physics has different forms. The earliest two are so called matrix mechanics [3] [4], which was formulated by a famous German physicist and a Nobel Prize winner Werner Heisenberg in 1925, and wave mechanics [2], which was formulated by an Austrian physicist and also a Nobel Prize winner Erwin Schrödinger in 1926. Later in 1930 Paul Dirac united these two theories into one by finding out that they are actually equivalent which was obviously a relief. Paul Dirac was a British physicist, who was awarded with the Nobel Prize along with E. Schrödinger. Dirac is also the inventor of the commonly used bra-ket notation which is a way to represent Hilbert space vectors and functionals that describe the quantum states. The reduced Planck constant $\hbar$ is also called Dirac constant because the shortened notation was invented by Dirac.[5] [6] The work of Heisenberg and Schrödinger is the basis of the most commonly used formalism although the notation has obviously changed and developed a bit when time has passed. The theory has also expanded a lot since those times and it has many new properties and applications.

In 1948 Richard Feynman derived an alternative way to describe quantum mechanics and this is called the path integral formulation [7]. In path integral theory the probability amplitude is a sum over all possible histories between the initial and final states. This relates to the action principle in classical mechanics and it is in fact a generalization of it. It also includes the solutions where time goes backwards. In figure 1 we can see three different paths the imaginary particle can choose from. Feynman derived his formulation by postulating three rules:

1. In the nature the events are probabilistic and the corresponding probability is P.

2. The probability P for an event is given by the complex square of the probability amplitude, Q. The quantum probability amplitude Q is the sum of all possible amplitudes q_h over all histories that lead to the event.

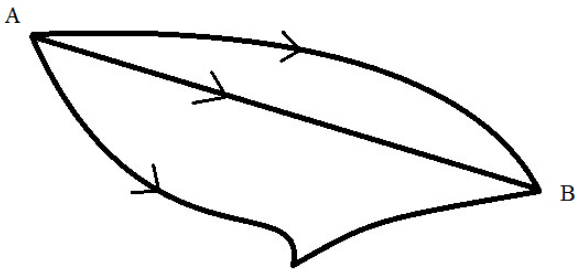

Figure 1: Example of three different paths that a particle can take going from point A to B.

3. The path is propotional to the classical action S time integral by $e^{iS/\hbar}$, where i is the imaginary unit and $\hbar$ is the reduced Planck constant.

Feynman's way of defining path integral approach in quantum theory opened new doors. It for example eventually enabled a connection to stochastic processes. This was used to unite the quantum field theory and statistical field theory together. So by choosing a specific formulation we can look at certain things from another perspective. This really shows the beauty of mathematics. In a way you could describe this to be a way of looking into things. But of course when it comes to matters like the quantum theory, you will have to invent a whole new way of thinking. After that you have to formulate the theory with the new approach. The quantum theory has certain postulates that have to be covered by the formalism in order it to be physically relevant. All in all it is eventually the physical reality that defines what type of mathematics you will be able to use. They have to describe the quantum reality. Through history there has been a lot of debate how to actually interpret these formalisms. We are also lacking the connection between the quantum world and the relativistic theory of gravity. So we will most certainly see new theories in the future.[8]

In this work our study first focuses on two potentials which are confined in an infinite well. First we have a linear potential and then an inverted oscillator potential. We will solve the energy eigenvalues and eigenfunctions using different methods. The equations are not solvable by using only analytic methods so we will present some numerical calculations and approximations as well. The equations of the linear potential are solved with two different boundary conditions. The first one is the normal boundary condition where the wave function goes to zero in the edge of the wall. The second one is a derivative boundary where the derivative of

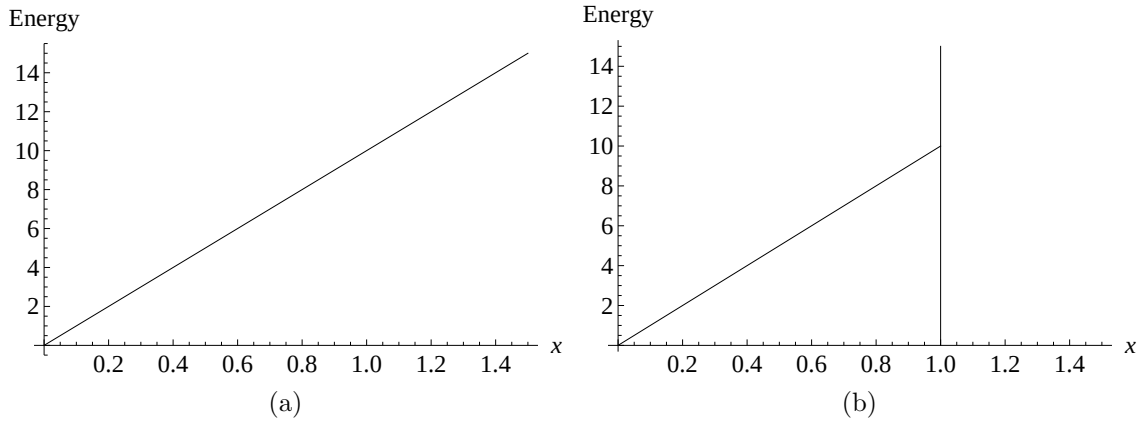

Figure 2: The similarity of two potentials. (a) The Flügge case where we have the linear potential with an infinite wall on the left side. (b) The linear potential with an infinite wall on both the left and the right side.

the wave function goes to zero in the edge and then we have either a maximum or minimum on the sides of the well. The inverted oscillator is solved only for the normal boundary conditions. After we have presented the solutions for these we study the tunneling properties. The study of the tunneling properties is done via Feynman's path integral theory. There we will find the instanton solution for the inverted oscillator potential in an infinite well.

Our study lays bases on the study of spin waves, especially in the experiments [9], [10] and [11]. The reason we have selected these potentials thus connects to the experimental work. The introduction of the derivative boundaries actually gives us the spin wave solutions. We want to introduce also the normal boundary conditions so that it is easier to compare them to the more unusual derivative boundaries. In general literature the derivative boundaries have been mostly left out and by that it is also an interesting field of study. By introducing both of them it is convinient to check out their similarities and differences side by side. For the inverted oscillator case we will look for the instanton solution. Usually the instanton solution is done for a double-well potential which is relatively similar to the inverted oscillator when the oscillator is in the infinite well.[8]

We will compare our linear potential results to a case studied in particle physics which included only the left side wall. The study of S. Flügge and his results are compared.[12] The comparison of the actual potentials can be seen in Figure 2, where Figure 2a refers to the potential where we only have one wall on the left side and Figure 2b refers to the potential where we have two walls on both sides.

The double-well potential consists of one hill and two wells next to it on both

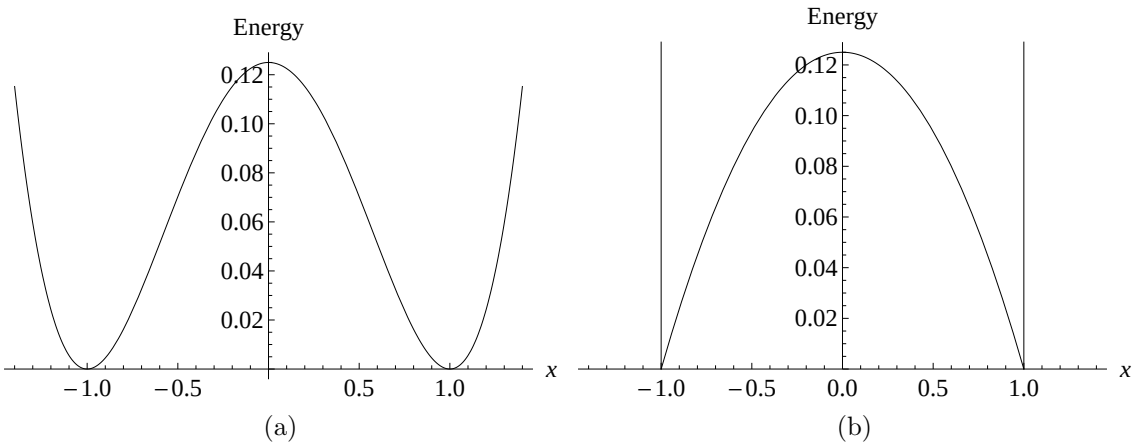

Figure 3: The similarity of two potentials. (a) The double-well potential. (b) The inverted oscillator potential in an infinite well.

sides, and it can be seen in Figure 3a. The inverted oscillator confined in a box looks basically same but the edges are sharp and walls are straight, which is seen in Figure 3b. The similarity of interest rises from the fact that the double-well potential has been studied a lot in the Bose-Einsten condensation.[13] In the experiments of our interest [9] and [11], we also see a study of the behaviour of the Bose-Einstein condensation. The first one is a case where the potential has a double well structure. The second one is related to quasiparticles in atomic hydrogen gas. Bose-Einstein condensation is related to experiments with real particles. Bose-Einstein condensation is low temperature state where a vast number of particles is at the lowest possible energy level. The particles can be thought of as a macroscopic ensemble and the ensemble starts to obey the rules of the quantum theory. The particles have to be bosons and they have to obey the Bose-Einstein statisctics. Boson is an elementary particle that does not obey the Pauli exclusion principle. So there are no restrictions on how many boson particles can occupy the same quantum state. The spin of a boson is an integer. The spin of a fermion, e.g. electron, is a half-integer. Fermions on the other hand must obey the Pauli exclusion principle. The condensate was named after the research of S.N. Bose and A. Einstein in the mid 1920's. [14]

The spin itself is a property of the elementary particles. It does not possess a counterpart model in the classical mechanics so it really is only a quantum phenomenon. The spin quantum number s is either an integer or half-integer. The spin

angular momentum S is a quantized property and it is defined as

$$S = \hbar\sqrt{s(s+1)} \tag{5}$$

where s is the spin quantum number.

The closest analogy to the spin is the angular momentum, i.e. a particle rotating around its axis. Spin waves in a quasiparticle interpretation are called magnons. In a crystal lattice it is the electrons' spin's collective excitation. So in other words the magnon represents a quantized electron spin wave. Its real particle counterpart is a boson which is related to the Bose-Einstein condensation. A quasiparticle is like a virtual particle. It is not a real particle like e.g. electron. It is more like a disturbance in a matter which behaves like a particle.[15] It can be thought of like a bubble in a glass of Coca Cola. It is an independent object inside the liquid eventhough it is basically only a ball that is formed because of the carbonic acid. It can move, collide with other bubbles, float on the surface etc. Still it has certain properties like its form, size, energy and momentum. By doing so they can be thought of as individual particles with a specific label on them. The same goes for quasiparticles. Besides magnon, there are also other quasiparticles like phonon, exciton, polaron, roton, plasmariton and plasmon. But what the spin waves actually are?

The spin wave is a group effect. From de Broglie's rule we know that particles can behave like a wave, where the wave length λ is given by

$$\lambda = \frac{h}{p}, \tag{6}$$

where h is the Planck constant and p is the momentum of the particle.[16] If you turn this around, you will end up with a wave that behaves like particle. We need to look deeper into the theory of electromagnetism but let us still stay away from the actual mathematical formalism. Like we said the spin can be classicly thought of as an angular momentum. If an electron rotates, it produces a small dipolar magnetic field pointing along the rotational axis. Let us assume we have atoms arranged in a periodical lattice in a crystalline material. The atoms are arranged so that they possess the electron spin 1/2 and have a magnetic moment. Now a ferromagnetic substance is a so called permanent magnet which is magnetic eventhough there is no externally applied magnetic field. If we have a ferromagnet, the magnetic momenta are parallelly aligned. This requires that the temperature is below the Curie temperature. If the temperature goes over the Curie temperature, the ferromagnet will turn into a paramagnet. We will introduce a strong external

magnetic field and the magnetic moments in our ferromagnetic crystal will now align parallel to it. Magnetic moments also produce a small magnetic field. Diverting the equilibrium positions of some of the magnetic moments will have an effect on the nearest magnetic moments. Again when the nearby magnetic moments are diverted a bit, they will have an affect on their neighbour magnetic moments. From this we get a propagated wave produced by the electron spins that moves around the crystal. This is the spin wave. When the spin is deflected, it does not go straight back to its equilibrium position. It will start to precess around the external magnetic field which was applied. The precession frequency is one of the important features of the spin waves. The precession will not last forever. The precession causes the atoms to vibrate in the lattice and from this we will see heat. So the spin wave will eventually turn into heat after time goes by.[15]

The study we have here is related to a dense gas of spin polarized atomic hydrogen. It differs from the ferromagnet where the basis is in the strong exchange interaction of the electrons. Now the weak exchange interraction is the key when it comes to the quantum gases that have identical atoms. From this we will have the identical spin rotation effect where the spin wave is actually result of the colliding identical spin rotations.[11] In atomic hydrogen gas we can encounter the identical spin rotation (ISR) effect which causes the excitation of spin waves.[20] [21] It is due to the weak interraction within the gas and it is a short event during collisions. The ISR effect causes the spin excitations to propagate. After a series of ISR collisions we will observe the spin waves in the more macroscopic scale. The subject has been studied also in [17], [18] and [19]. In our case of interest it is the magnetic field that becomes the quantum potential. We will just quickly show what we are going for and we do not go into details with this one. The complex diffusion equation for the spin transport, with spin polarization $S_+ = S_x + iS_y$, is

$$i\frac{\partial S_+}{\partial t} = D_0\frac{\epsilon}{\mu}\nabla^2 S_+ + \gamma\delta B_0 S_+, \tag{7}$$

where D_0 is the spin diffusion coefficient in the unpolarized gas, $\epsilon = 1$ for bosons, $\epsilon = -1$ for fermions, γ is the gyromagnetic ratio, and δB_0 is the magnetic field deviation from the average value B_0. The main magnetic field is of course in z direction and the spins will precess around it. We define the effective mass of the particle

$$m^* = -\frac{\hbar\mu}{2D_0\epsilon}. \tag{8}$$

We get a wave equation that resembles the Schrödinger equation (3) quite a lot when we rearrange it and multiply it with Dirac constant $\hbar$

$$-\frac{\hbar^2}{2m^*}\nabla^2 S_+ + \hbar\gamma\delta B_0 S_+ = i\hbar\frac{\partial S_+}{\partial t}. \tag{9}$$

The potential term in here is thus

$$V_{spin} = \hbar\gamma\delta B_0. \tag{10}$$

The reason for this is that δB_0 is inhomogeneous and therefore it is dependent from the spatial components so that we can view it as a potential well. By different selections of the parameters of the magnetic field we get our cases - the linear potential and the inverted oscillator potential in an infinite well. In other words we can achieve this by adjusting δB_0. The adjustments can actually be done during the experiments. So the parameters are not just some fixed values that happen to show up with this behaviour. They can be altered and tested with higher or lower slopes by adjusting the parameters of the external fields. It is also very important to note that our study is done in a situation which is simplified to a 1-dimensional case. The actual experiments are 3-dimensional. There we have the resemblance of a toroid potential corresponding to the inverted oscillator and a linear magnetic field corresponding to the linear potential.

In the experiments our main magnetic field is in the z-direction and it causes a toroidal counter magnetic field on the edge of the cylinder. The toroid is in the xy-plane and a simplified cross section of the toroid is an inverted oscillator. The resemblance of the toroidal shape comes from the impurities of the surrounding material. The material inside the cylinder is spin polarized atomic hydrogen. By using and adjusting inductors it is possible to create a linear magnetic potential in the z-direction. If the inductors are strong enough, the linear potential dominates. This is why it is notable to check out the toroid potential and linear potential separately. It is also possible to do them at the same time. Furthermore, it is possible to cancel the toroid potential completely using the inductors.

The resemblance between the inverted oscillator in an infinite well and the double well potential leads us also to the possibility of tunneling. The idea of the quantum tunneling is an interesting point of view which is also a thing that does not happen in our macroscopically observed every day life. It is still a fact delivered by the quantum theory. Historically the tunneling is attached with the double well potential because the theory of tunneling emerged when F. Hund studied the properties of the double

well potential in 1927. He noticed that there exists a probability of the electron penetrating through a classically forbidden barrier inside an atom.[22] Friedrich Hund was a German physist who specialized in the study of nuclear physics. He was an assistant to the famous German physicist Max Born. It was also Born that realized that the quantum tunneling is a ground breaking part of the theory itself, and was awarded with the Nobel prize in physics in 1954 for his work on quantum mechanics. One way to interprete the tunneling probability amplitude is the way to to explore the instanton solution. This is what we want to compare to the results of the inverted oscillator in an infinite well.

One of the purposes of this work is also to give a short introduction for using different special functions. A little knowledge on how they are used, what different forms they have and how do they look like. For this we will show some basic properties and methods. Special functions are a class of mathematical functions that usually have a certain name and this is because they have been used in some field of study. The names have been given mostly for historical reason and are offen referred to the first person who studied or solved them. The names also differ in different references. In some they are used by their general name and in some a specific subgroup may have a name of its own. There is no specific definition for what counts as a special funtion. It is more of a list of silently agreed functions. Lots of books and tables have been made about their properties, connections, solutions, usage etc. One of the most referred book is Handbook of Mathematical Functions by M. Abramoviz and I.A. Stegun [23], to which we also mainly refer. We will concentrate on *Airy functions* and *parabolic cylinder functions* because they are an essential part of the given solutions in our problems. We have also added some interesting historical points of both the physical theory and the people behind it.

2 Infinite well with a linear potential

2.1 Airy functions

We first examine a 1-dimensional quantum system that is in an infinite well with a linear potential of the form

$$V(x) = kx \tag{11}$$

and solve its energy eigenvalues and eigenfunctions. We will have an adjustable potential parameter k and boundaries on both sides for the well. The solutions for this type of differential equations are called Airy functions which are named after the British astronomer and mathematician George Biddel Airy who investigated these in the 19th century [24]. G.B. Airy was especially established in the research of orbiting planets and was close to being the first recognized discoverer of the planet Neptune. In 1851 he also got the honor of defining that the prime meridian goes through the location of the Greenwich's Royal Observatory. Later his definition was chosen for the definition of the prime meridian worldwide. The actual differential equations we are investigating here got the attention of G.B. Airy when he was studying optics.[25] The Airy functions are actually a special case of a larger group of functions called the Bessel functions. Airy function is a representation of a certain order Bessel function. It is a 1/3 fractional Bessel function.[23] The Bessel functions were first introduced by David Bernoulli and also investigated by J.L.L. Lagrange, L. Euler and S.D. Poisson among others. Later on in 1824 Friedrich Bessel generalized and rearranged the equations more precisely.[26]

During the investigations of the properties of special functions like the Airy functions we refer to [23]. There are plenty of relations and properties that give us the possibility to present these functions in a different form. The Airy functions come in the form of two, $Ai(x)$ and $Bi(x)$. They are linearly independent solutions for the differential equation

$$y'' - xy = 0 \tag{12}$$

and the solution is in the form

$$y(x) = AAi(x) + BBi(x). \tag{13}$$

These can also be written

$$Ai(x) = c_1 f(x) - c_2 g(x) \tag{14}$$
$$Bi(x) = \sqrt{3}(c_1 f(x) + c_2 g(x)) \tag{15}$$

where the functions $f(x)$ and $g(x)$ are

$$\begin{aligned} f(x) &= 1 + \frac{1}{3!}x^3 + \frac{1\cdot 4}{6!}x^6 + \frac{1\cdot 4\cdot 7}{9!}x^9 + \dots \\ &= \sum_{i=0}^{\infty} 3^i \left(\frac{1}{3}\right)_i \frac{x^{3i}}{(3i)!} \end{aligned} \tag{16}$$

$$\begin{aligned} g(x) &= x + \frac{2}{4!}x^4 + \frac{2\cdot 5}{7!}x^7 + \frac{2\cdot 5\cdot 8}{10!}x^{10} + \dots \\ &= \sum_{i=0}^{\infty} 3^i \left(\frac{2}{3}\right)_i \frac{x^{3i+1}}{(3i+1)!} \end{aligned} \tag{17}$$

and

$$\left(z + \frac{1}{3}\right)_0 = 1 \tag{18}$$
$$3^i \left(z + \frac{1}{3}\right)_i = (3z+1)(3z+4)\cdots(3z+3i-2) \tag{19}$$

where $k = 1, 2, 3, \dots$and z is an arbitrary number. The factors c_1 and c_2 can be written

$$c_1 = Ai(0) = \frac{Bi(0)}{\sqrt{3}} = \frac{3^{-2/3}}{\Gamma(2/3)} \tag{20}$$
$$c_2 = -Ai'(0) = \frac{Bi'(0)}{\sqrt{3}} = \frac{3^{-1/3}}{\Gamma(1/3)} \tag{21}$$

In (20) and (21) we have the Gamma function $\Gamma(\alpha)$ where $\alpha \in \mathbb{C}$. There are also certain relations between the Airy functions $Ai(x)$ and $Bi(x)$. Let us have a brief look at those as well. Two identities to begin with are

$$Ai(x) + e^{\frac{2\pi i}{3}} Ai(xe^{\frac{2\pi i}{3}}) + e^{-\frac{2\pi i}{3}} Ai(xe^{-\frac{2\pi i}{3}}) = 0 \tag{22}$$
$$Bi(x) + e^{\frac{2\pi i}{3}} Bi(xe^{\frac{2\pi i}{3}}) + e^{-\frac{2\pi i}{3}} Bi(xe^{-\frac{2\pi i}{3}}) = 0. \tag{23}$$

Let us prove the first one (22) briefly. It is easily calculated when we substitute (14), (15), (16) and (17) into (22). We also need to use the Euler's formula which

states that

$$e^{ix} = \cos(x) + i\sin(x). \tag{24}$$

Having all of these we end up calculating the factors and series in the form

$$\begin{gathered}
Ai(x) + e^{\frac{2\pi i}{3}} Ai(xe^{\frac{2\pi i}{3}}) + e^{-\frac{2\pi i}{3}} Ai(xe^{-\frac{2\pi i}{3}}) = \\
c_1\left(1 + \tfrac{1}{3!}x^3 + \tfrac{4}{6!}x^6 + \ldots\right) - c_2\left(x + \tfrac{2}{4!}x^4 + \tfrac{10}{7!}x^7 + \ldots\right) \\
e^{\frac{2\pi i}{3}} c_1\left(1 + \tfrac{1}{3!}x^3 e^{\frac{2\pi i}{3}\cdot 3} + \tfrac{4}{6!}x^6 e^{\frac{2\pi i}{3}\cdot 6} + \ldots\right) \\
-e^{\frac{2\pi i}{3}} c_2\left(x + \tfrac{2}{4!}x^4 e^{\frac{2\pi i}{3}\cdot 4} + \tfrac{10}{7!}x^7 e^{\frac{2\pi i}{3}\cdot 7} + \ldots\right) \\
e^{-\frac{2\pi i}{3}} c_1\left(1 + \tfrac{1}{3!}x^3 e^{-\frac{2\pi i}{3}\cdot 3} + \tfrac{4}{6!}x^6 e^{-\frac{2\pi i}{3}\cdot 6} + \ldots\right) \\
-e^{-\frac{2\pi i}{3}} c_2\left(x + \tfrac{2}{4!}x^4 e^{-\frac{2\pi i}{3}\cdot 4} + \tfrac{10}{7!}x^7 e^{-\frac{2\pi i}{3}\cdot 7} + \ldots\right).
\end{gathered}$$

First we notice that $e^{\frac{2\pi i}{3}\cdot n} = 1$, where $n = 3, 6, 9, 12, \ldots$, which means that the bracket phrases having a factor c_1 are the same. After using Euler's formula (24) we get for those that

$$\begin{gathered}
c_1(\ldots) + \left(\cos(\tfrac{2\pi}{3}) + i\sin(\tfrac{2\pi}{3})\right) c_1(\ldots) + \left(\cos(\tfrac{2\pi}{3}) - i\sin(\tfrac{2\pi}{3})\right) c_1(\ldots) = \\
c_1(\ldots) - \tfrac{1}{2}c_1(\ldots) - \tfrac{1}{2}c_1(\ldots) = 0
\end{gathered}$$

where we have used that $\cos(\frac{2\pi}{3}) = -\frac{1}{2}$. So now we have got ridden of the terms that contain the coefficient c_1. Now we will rip open the rest. For simplicity we will leave out the coefficient c_2 because it is in front of every term. Focus is in the first term inside the round brackets which has a coefficient x. The other terms will behave in a same way. We will also use the following markings $\cos(2\pi/3) \to c$ and $\sin(2\pi/3) \to s$. We get

$$\begin{aligned}
-x - [c+is]x[c+is] - [c-is]x[c-is] &= \\
-x - x(c^2 + 2ics - s^2) - x(c^2 - 2ics - s^2) &= \\
-x - 2x\left(c^2 - s^2\right) &= \\
-x - 2x\left(\left(-\frac{1}{2}\right)^2 - \left(\frac{\sqrt{3}}{2}\right)^2\right) &= \\
-x - 2x\left(-\frac{1}{2}\right) &= 0.
\end{aligned}$$

In this way we end up to the identity (22). In a similar way it can be proven that between the solutions $Ai(x)$ and $Bi(x)$ we have a relation

$$Bi(x) = e^{\frac{\pi i}{6}} Ai(xe^{\frac{2\pi i}{3}}) + e^{-\frac{\pi i}{6}} Ai(xe^{-\frac{2\pi i}{3}}). \tag{25}$$

which might be of use in some situations.

The integral representation for the Airy functions can be written in the form

$$(3a)^{-1/3}\pi Ai\left(\pm(3a)^{-1/3}x\right) = \int_0^\infty \cos(at^3 \pm xt)dt \tag{26}$$

$$(3a)^{-1/3}\pi Bi\left(\pm(3a)^{-1/3}x\right) = \int_0^\infty \left(e^{-at^3 \pm xt} + \sin(at^3 \pm xt)\right) dt. \tag{27}$$

The Airy functions can also be represented in terms of other special functions. Let us present them in terms of the Bessel functions. First we of course need to tell and define what the Bessel functions are. The Bessel functions are the solution to the following differential equation

$$x^2\frac{d^2y}{dx^2} + \frac{dy}{dx} + (x^2 - n^2)y = 0. \tag{28}$$

The Bessel functions also satisfy the recurrence formulas

$$\frac{2n}{x}Z_n(x) = Z_{n+1}(x) + Z_{n-1}(x) \tag{29}$$

and for the derivation

$$-2\frac{dZ_n(x)}{dx} = Z_{n+1}(x) + Z_{n-1}(x). \tag{30}$$

There are three types of the functions that give solutions to the equation (28). The Bessel functions of the first kind $J_{\pm n}(x)$, the second kind $Y_n(x)$ and the third kind $H_n^{(2)}(x)$, $H_n^{(1)}(x)$. The second kind Bessel functions are also known as Weber's functions, and the third kind Bessel functions are also known as Hankel functions. We will present the series definition to the first kind of the Bessel functions $J_n(x)$ because we need only that to our original purpose which was to present the Airy functions in terms of the Bessel functions

$$J_n(x) = \left(\frac{x}{2}\right)^n \sum_{k=0}^{\infty} \frac{(-\frac{1}{4}x^2)^k}{k!\Gamma(n+k+1)}, \tag{31}$$

where Γ is the Gamma function. The Bessel functions are also in some literature

referred as cylinder functions. In Chapter 3 we will discuss about parabolic cylinder functions. The Bessel functions can also be linked to those which we will get back later.

First for the representation of the Airy function in the terms of the Bessel function we will define that our variable

$$\xi = \frac{2}{3}x^{3/2}. \tag{32}$$

For the function $Ai(x)$ we have

$$\begin{aligned} Ai(x) &= \frac{1}{3}\sqrt{x}\left(I_{-1/3}(\xi) - I_{1/3}(\xi)\right) \\ &= \frac{1}{\pi}\sqrt{\frac{x}{3}}K_{1/3}(\xi) \end{aligned} \tag{33}$$

and

$$\begin{aligned} Ai(-x) &= \frac{1}{3}\sqrt{x}\left(J_{-1/3}(\xi) + J_{1/3}(\xi)\right) \\ &= \frac{1}{2}\sqrt{\frac{x}{3}}\left(e^{i\pi/6}H^{(1)}_{1/3}(\xi) + e^{-i\pi/6}H^{(2)}_{1/3}(\xi)\right). \end{aligned} \tag{34}$$

For the derivative of the function $Ai(x)$

$$\begin{aligned} Ai'(x) &= -\frac{1}{3}\sqrt{x}\left(I_{-2/3}(\xi) - I_{1/3}(\xi)\right) \\ &= -\frac{x}{\pi\sqrt{3}}K_{2/3}(\xi) \end{aligned} \tag{35}$$

and

$$\begin{aligned} Ai'(-x) &= -\frac{1}{3}x\left(J_{-2/3}(\xi) - J_{2/3}(\xi)\right) \\ &= \frac{x}{2\sqrt{3}}\left(e^{-i\pi/6}H^{(1)}_{2/3}(\xi) + e^{i\pi/6}H^{(2)}_{2/3}(\xi)\right). \end{aligned} \tag{36}$$

In a similar way for the other Airy function $Bi(x)$

$$Bi(x) = \sqrt{\frac{x}{3}}\left(I_{-1/3}(\xi) + I_{1/3}(\xi)\right) \tag{37}$$

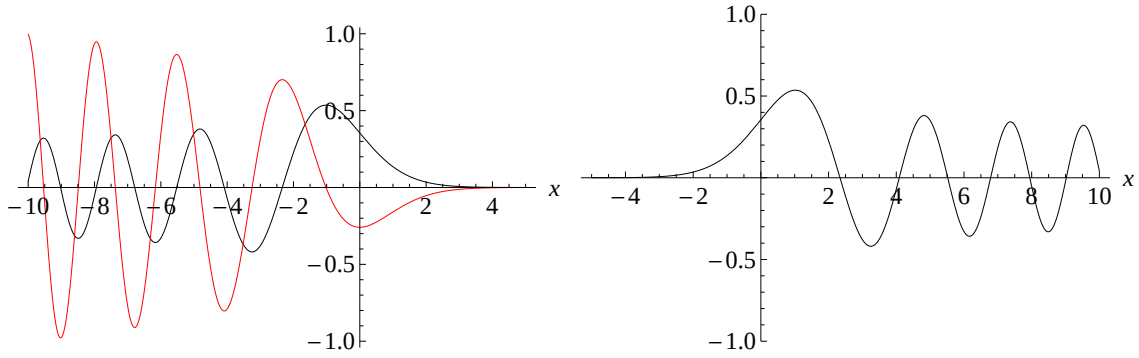

(a) (b)

Figure 4: Airy function $Ai(x)$. (a) The black curve is $Ai(x)$ and the red curve is $Ai'(x)$. (b) $Ai(-x)$.

and

$$\begin{aligned} Bi(-x) &= \sqrt{\frac{x}{3}}\left(J_{-1/3}(\xi) - J_{1/3}(\xi)\right) \\ &= \frac{i}{2}\sqrt{\frac{x}{3}}\left(e^{i\pi/6}H^{(1)}_{1/3}(\xi) - e^{-i\pi/6}H^{(2)}_{1/3}(\xi)\right). \end{aligned} \tag{38}$$

For the derivative of the function $Bi(x)$

$$Bi'(x) = \frac{x}{\sqrt{3}}\left(I_{-2/3}(\xi) + I_{2/3}(\xi)\right) \tag{39}$$

and

$$\begin{aligned} Bi'(-x) &= \frac{x}{\sqrt{3}}\left(J_{-2/3}(\xi) + J_{2/3}(\xi)\right) \\ &= \frac{ix}{2\sqrt{3}}\left(e^{-i\pi/6}H^{(1)}_{2/3}(\xi) - e^{i\pi/6}H^{(2)}_{2/3}(\xi)\right). \end{aligned} \tag{40}$$

It is also to be noted that in some literature you can see the Airy functions named as $Gi(x)$ and $Hi(x)$. It is just a different formulation and nothing else. The relation is just a transformation away from our notation of $Ai(x)$ and $Bi(x)$. We do not go deeper into these matters.

In Figure 4 you can see how the Airy function $Ai(x)$ and its derivative $Ai'(x)$ behave. If you compare Figures 4a and 4b, you can see that the Airy function $Ai(x)$ is mirror symmetric. In Figure 5 you can see in a similar way how the Airy function $Bi(x)$ behaves. The Figures 5a and 5b show that $Bi(x)$ is also mirror symmetric. The fundamental difference between $Ai(x)$ and $Bi(x)$ is in in the limits

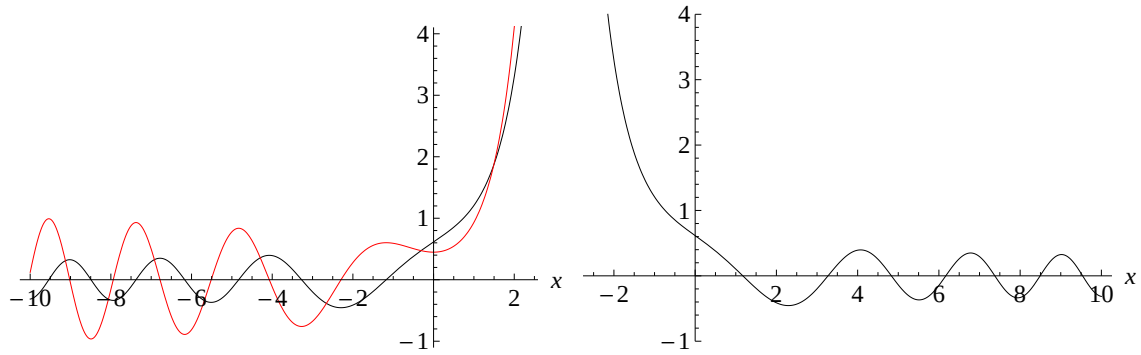

Figure 5: Airy function $Bi(x)$. (a) The black curve is $Bi(x)$ and the red curve is $Bi'(x)$. (b) $Bi(-x)$.

when $x \to \infty$. We have

$$\lim_{x\to\infty} Ai(x) = 0 \tag{41}$$

and

$$\lim_{x\to\infty} Bi(x) = \infty. \tag{42}$$

This is an important difference because it can be used to evaluate the solutions that are needed in certain problems. For example, if the boundary conditions require that the solution must go to zero at all times when $x \to \infty$, then we can rule out the $Bi(x)$ solution entirely. Then the corresponding wave function would only consist of the Airy function $Ai(x)$.

2.2 Solutions

2.2.1 Solving the Schrödinger equation

The linear potential has been studied for example in particle physics. [12] The study has been focused on the system where there is an infinite wall only on the other side. The potential can for instance be considered to describe the motion of a particle falling under gravity or an electron in a constant electric field of a capacitor. In this study we present the solution to the case where the system is bound from both sides. We also investigate alongside the situation where we have so called derivative boundaries. In the derivative boundary situation the wave function has either a minimum or a maximum on the sides of the walls. It does not go to zero like in

the case of the normal boundaries. The derivative boundaries are of special interest because their solutions are related to the spin wave solutions. As we discussed in Chapter 1 that by introducing the unusual boundaries, we can solve the equations for the propagating spin waves of the system. The potential itself is seen in Figure 2b.

Our motivation is to present both the normal and the derivative boundaries so that we will be able to compare them. We will plot figures and show tables that tell their similarities and differences. These are also compared to the traditional text book example, a particle in a box. We will see certain similarities to the plain box solution when the potential is small enough. We will refer to [23] with the solutions to the equations.

The Schrödinger equation for the system is

$$-\frac{\hbar^2}{2m}\psi''(x) + kx\psi(x) = E\psi(x), \tag{43}$$

when $x \in \{-0, L\}$ and zero elsewhere. We have the markings for the Dirac constant $\hbar$, mass m, wave function ψ, potential parameter k, position x and the corresponding energy E. We study this with two different boundary conditions in a box which has a length L. We will call the first ones as the normal boundary conditions

$$\psi(0) = \psi(L) = 0. \tag{44}$$

The second ones are called the derivative boundary conditions

$$\psi'(0) = \psi'(L) = 0 \tag{45}$$

where we have either a maximum or minimum on the sides of the well.

The solution for the Schrödinger equation (43) gives us a pair of Airy functions $Ai(x)$ and $Bi(x)$. If there were only one wall, we would be able to get rid of the other Airy function with the aid of boundary conditions and behavior of the Airy functions. In this case we will need both of the functions. We will first adjust the Schrödinger equation a bit before we present the Airy function solution. By changing the variable we get closer to what we want. We need a substitution which is in the form

$$\xi = \left(\frac{2mk}{\hbar^2}\right)^{1/3}\left(x - \frac{E}{k}\right). \tag{46}$$

By doing this we get the Schrödinger equation in the form

$$f'' - \xi f = 0 \tag{47}$$

which is the equation same as (12). We will show how this transformation is done and prove that it satisfies the original equation.

Our boundaries will be

$$\xi_0 = -\left(\frac{2m}{\hbar^2 k^2}\right)^{1/3} E \tag{48}$$

$$\xi_L = -\left(\frac{2mk}{\hbar^2}\right)^{1/3} \left(L - \frac{E}{k}\right). \tag{49}$$

So we will end up with

$$\begin{cases} aAi(\xi_0) + bBi(\xi_0) = 0 \\ aAi(\xi_L) + bBi(\xi_L) = 0 \end{cases} \tag{50}$$

which can also be written in a matrix form

$$\begin{pmatrix} Ai(\xi_0) & Bi(\xi_0) \\ Ai(\xi_L) & Bi(\xi_L) \end{pmatrix} \begin{pmatrix} a \\ b \end{pmatrix} = 0. \tag{51}$$

We can continue to modify (50) if we solve a from the upper row. We get that

$$a = -\frac{bBi(\xi_0)}{Ai(\xi_0)}. \tag{52}$$

Then by inserting this to the second row of (50), we get the equation

$$Ai(\xi_0)Bi(\xi_L) - Ai(\xi_L)Bi(\xi_0) = 0. \tag{53}$$

Now we need to find out the different energy values that satisfy the equation (53). Before we go into this, we will modify our equation to a dimensionless form. It is just a little trick that makes the calculations easier. To do this we will simply just define that the mass $m = 1/2$ and the Dirac constant $\hbar = 1$. So this is assumed later on in this section and when we refer to the previous equations, we do it with the above assumption. For solving the energy eigenvalues, we need some numeric tricks. This is shown in detail in Appendix A. Basically this is done by using the equation (50) from the boundary conditions.

We have the Schrödinger equation in the desired form and we can now use the knowledge from the Airy functions. The solution to our equation is

$$\psi_i(x) = a_i \cdot Ai\left[\frac{1}{k^{-2/3}}(kx - E_i)\right] + b_i \cdot Bi\left[\frac{1}{k^{-2/3}}(kx - E_i)\right] \tag{54}$$

where $i = 1, 2, 3, \ldots$ and it stands for the index of the eigenvalues. From the boundary conditions (50) we get the constant of integration b_i written in terms of a_i so that

$$b_i = -\frac{Ai(\xi_0)}{Bi(\xi_0)}a_i. \tag{55}$$

The other constant of integration a_i is accessible via normalization and it needs to be done separately for every energy eigenvalue. This is also shown in details in Appendix A. After the normalization is done, we have all the parameters. Now we are ready to start plotting different solutions and see how they behave.

2.2.2 Analysis

First we will analyze the situation if the Figure 6a where the potential parameter $k = 1$ and the box length $L = 1$. The situation is almost as the particle in the box in Figure 6a. The lowest energy state value is around $E_1 \approx 10$ so the potential does not really have any influence in it anymore. As you can see the wave functions behave like the trigonometric functions in the particle in the box solution. The first eigenfunction has one node, second has two, third has three etc. In this case the energy eigenvalues are closely matching the energy eigenvalues of the particle in a box. For the figures we have done some scaling in order to make the eigenfunctions appear more visually. In this case the three plotted eigenfunctions are five times larger in the sense of amplitude than they are suppose to be.

The derivative boundaries behave basically in the same manner as the normal boundaries in this case which can be seen in Figure 6b. The energy states are just much lower than functions of the the normal conditions which is interesting. The lowest energy state value here is as low as $E_1^D \approx 0.5$ as the second state is $E_2^2 \approx 10$ which was the situation for the first energy state with the normal boundary. The upper index D refers to the derivative boundary. The derivative boundaries do have one crucial difference already in the beginning. The first energy eigenstate does not have a node at all. It just converges towards zero when $x \to L$. From the second eigenstate onwards the behaviour is more like the one with the normal boundary

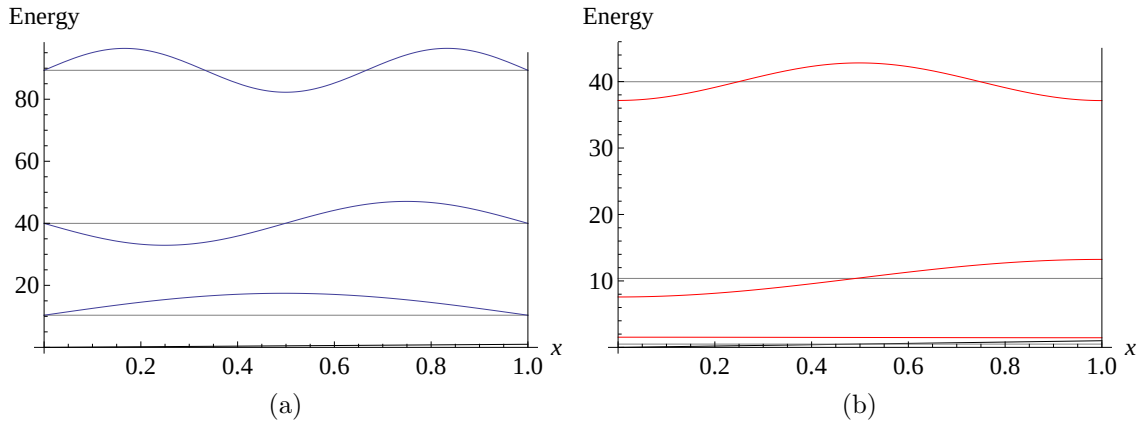

Figure 6: Energy eigenfunctions with the parameters $k = 1$ and $L = 1$. (a) Normal boundary conditions (44). (b) Derivative boundary conditions (45).

condition. The limit of the first eigenstate is seen better in the Figure 7b where we are looking at the situation when $k = 50$ and $L = 1$. In Figure 6b the scaling multiplier is 3 and especially the property of the first energy eigenstate is not seen that clearly.

It is noticeable that the first energy eigenstate of the derivate boundary is not a constant. From Figure 6b it might seem so. This could in a principle happen if there were no potential. So for the particle in a box it is a solvable case that the energy eigenstate is a constant. This only applies when we are dealing with the derivative boundaries. This does not work for the normal conditions regardless of our potential. The reason it does not work is that the Schrödinger equation will not carry out its requirements.

The case $k = 50$ and $L = 1$ with the normal boundary is in Figure 7a. On the lowest energy level there exists a possibility that the particle can be in the classically forbidden area. Then the particle would be on the other side of the quantum potential. The wave function encounters the potential barrier at $x \approx 0.66$. We can now calculate the probability that the particle can be found on the other side of the barrier. The probability that the particle will be in a region $a \leq x \leq b$ is the integral of the probability density over this region

$$P_{a \leq x \leq b} = \int_a^b |\psi(x)|^2 dx \tag{56}$$

assuming that the wave function is a measurable Hilbert space functional, $\psi \in$

$L^2(\Re)$.[12] In this case substituting our values we get

$$P^{E_1}_{0.66\leq x\leq 1} = 7.4\%$$

where the upper index refers to the energy state we are dealing with. Just in case we will check that we get the right result by calculating the counterpart

$$P^{E_1}_{0\leq x\leq 0.66} = 92.6\%.$$

These two equal

$$P^{E_1}_{0.66\leq x\leq 1} + P^{E_1}_{0\leq x\leq 0.66} = 100\%$$

as they should according to the probability calculus. But the really interesting part here is that there is a 7.4% chance that the particle in our system is tunneling through the barrier in the first energy level. The second energy level is already above the potential barrier so there is no possibility for going through the barrier to the classically forbidden area. It is also interesting to notice that the potential parameter k is already 50 times larger than the box length L, and we only have one energy state colliding with the potential barrier. Also on the second energy state the particle is more likely to be on the right side which is also interesting and can be seen in Figure 7a, where $E_2 \approx 115$. After that the behavior of the energy eigenfunctions is more balanced and starts to resemble the case of the particle in a box. We must also add that due to the free choice of the function sign being positive or negative, we choose the sign of the 4th eigenstate of the normal boundary conditions to be negative so that the results would be consistent with the others.

The derivative boundaries in the case $k = 50$ and $L = 1$ are shown in the figure 7b. We have two energy eigenfunctions colliding with the potential barrier. Although the second state barely touches the barrier end. We can clearly see that the first energy eigenstate does not have a zero point. There also exists a possibility that the particle is found in the classically forbidden area. Here the scaling multiplier is 7.

The next in the line of progress is the case $k = 150$ and $L = 1$ which can be looked upon from Figure 8. We want to show how the wave function evolves when the potential parameter k is much higher than the length of the box L. By doing this step by step it is easy to show what happens during the process. As you can see the situation with the normal boundary conditions in Figure 8a that the energy

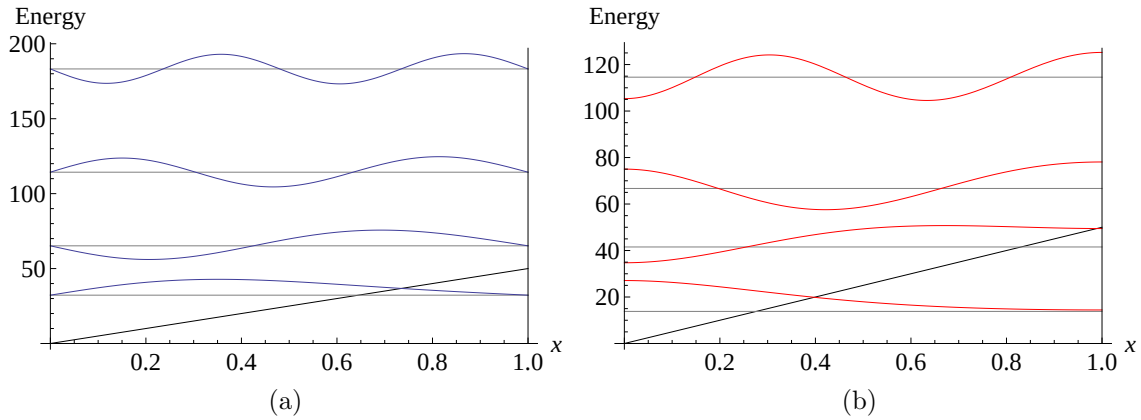

Figure 7: Energy eigenfunctions with the parameters $k = 50$ and $L = 1$. (a) Normal boundary conditions (44). (b) Derivative boundary conditions (45).

eigenvalues are already much higher than in the case of $k = 50$. Here we have two of the lowest energy eigenfunctions colliding with the potential barrier. We can calculate the probabilities for the particle tunneling through the barrier. The first energy eigenfunction crosses the barrier approximately at $x \approx 0.44$. That means that it has the probability

$$P^{E_1}_{0.44 \leq x \leq 1} = 12.6\%. \tag{57}$$

For the second energy eigenfunction the crossing is at $x \approx 0.78$ and the probability is calculated in a bit smaller region

$$P^{E_2}_{0.78 \leq x \leq 1} = 5.3\%. \tag{58}$$

So it can be seen from these that it is an actual and exciting possibility for the particle to enter our potential barrier. If the particle is on the classically forbidden area, it is most probable for it to be in the close vicinity of the barrier. For the first eigenfunction this is easy to compare to (57), if we check only the area $0.44 \leq x \leq 0.65$, the probability is

$$P^{E_1}_{0.5 \leq x \leq 0.65} = 11.5\%. \tag{59}$$

We can see that the results in (57) and (59) are almost the same as they differ from each other for about one percentage unit. This means that the particle is likely to be close to the barrier even though it is on the other side.

Then we start to look at Figure 8b. The derivative boundary situation has

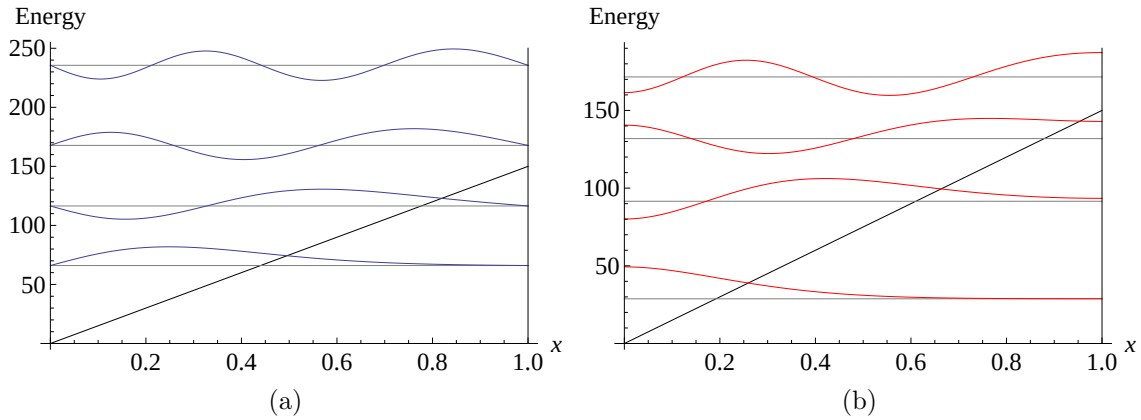

Figure 8: Energy eigenfunctions with the parameters $k = 150$ and $L = 1$. (a) Normal boundary conditions (44). (b) Derivative boundary conditions (45).

again much smaller energy eigenvalues and already three eigenfunctions are able to penetrate the potential barrier. Once again we can also see that the lowest energy only converges towards the energy value. Beginning from the second energy state we start to see the node behavior similar to the normal boundary. We can compare the probability results to the normal boundary by calculating the probabilities for the first two energy states. The first energy state crosses the barrier at $x \approx 0.20$ which is at a very early stage as it is expected due to the low energy values. The probability for the classically forbidden area is

$$P^{E_1^D}_{0.20 \leq x \leq 1} = 20.8\% \tag{60}$$

where the upper index E_1^D refers to the first energy eigenstate with the derivative boundary. This is already a quite substantial probability for the particle to be on the classically forbidden area. If we look at a smaller area like in (59), we get

$$P^{E_1^D}_{0.20 \leq x \leq 0.5} = 20.4\%. \tag{61}$$

This sends us a very strong message that the particle is to be found next to the barrier also on the classically forbidden area. The second energy state crosses the barrier at $x \approx 0.62$ and the probability is

$$P^{E_2^D}_{0.62 \leq x \leq 1} = 12.0\% \tag{62}$$

which is approximately the same as for the first energy state in the normal boundary (57).

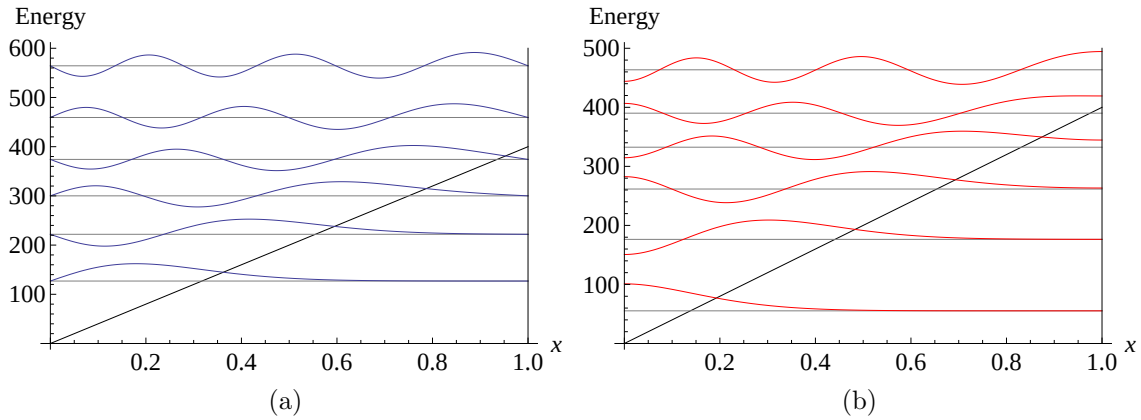

Figure 9: Energy eigenfunctions with the parameters $k = 400$ and $L = 1$. (a) Normal boundary conditions (44). (b) Derivative boundary conditions (45).

The situation remains quite similar when $k = 400$ and $L = 1$ as can be seen from Figure 9. The amount of the energy eigenfunctions that are able to penetrate the potential increase which is of course expectable. The behavior is very similar to the previous cases and again as the energy levels rise, they start to resemble the case of the particle in a box. From this we are quite assured that the behavior is secured to be like this for a while. Now we raise the bar and go straight to a violently larger scale. In our experimental background the barrier slope is much greater than the box length so let us see through the ultimate difference.

Before we go into the very deep potential we will shortly look at the box at a different size than $L = 1$. This is just to be sure that the behavior looks the same as it did when $L = 1$. First we have the case where $k = 3$ and $L = 2$ which is presented in Figure 10. The situation looks quite similar to the case of $k = 50$ and $L = 1$ which is seen in Figure 7. In the normal boundary conditions there is the lowest energy eigenstate that collides with the potential barrier. The energy values are much lower than in Figure 7. It seems that widening the box lowers the energy values quite a bit. This makes it possible for the lowest energy eigenfunctions to have the possibility to be on the classically forbidden area with the potential barrier. In the derivative boundaries the same asymptotic behavior is seen on the first eigenstate and the rest behave similarly to the previous.

When the box is made even wider, the energies decrease even more. This is seen when $k = 4$ and $L = 5$ which is the case in Figure 11. In the situation of the normal boundary conditions we have four lowest energy eigenstates that are able to penetrate the potential barrier. For the derivative boundary the number of the penetrating energy states is five.

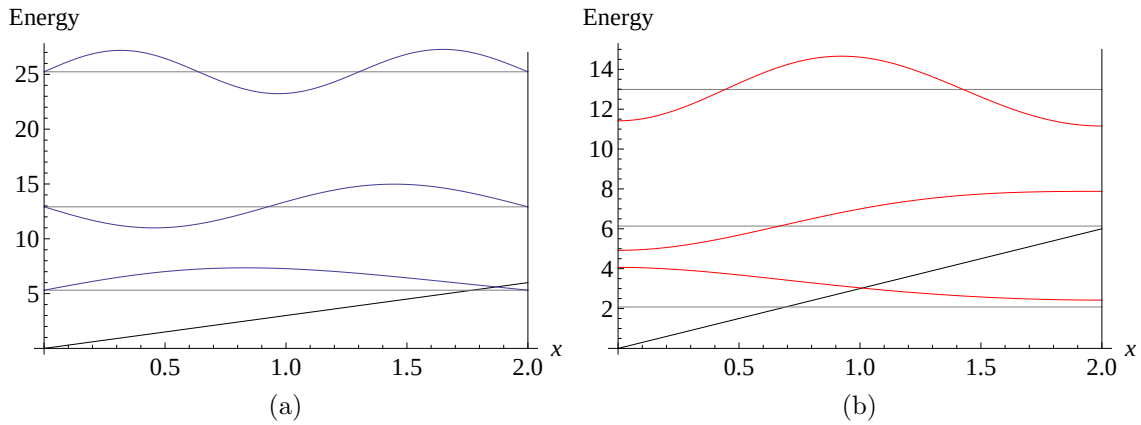

Figure 10: Energy eigenfunctions with the parameters $k = 3$ and $L = 2$. (a) Normal boundary conditions (44). (b) Derivative boundary conditions (45).

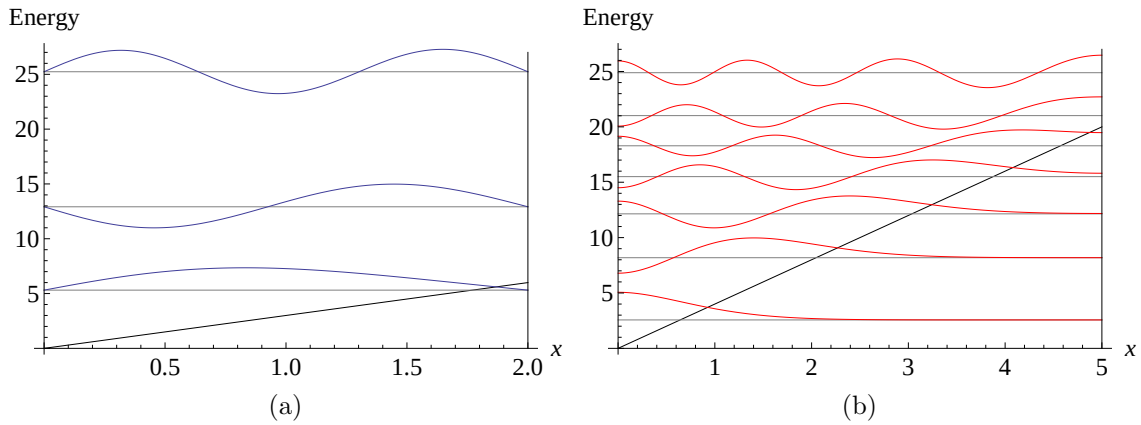

Figure 11: Energy eigenfunctions with the parameters $k = 4$ and $L = 5$. (a) Normal boundary conditions (44). (b) Derivative boundary conditions (45).

One of the things we can see going through all these different cases is that the wave functions seem to have concentrated more densely in the left side. This is seen in both the normal and the derivative boundary. The dense concentration here means that the nodes are more closely together the further to the left side you look. This can be seen especially well for example in Figure 11a. In terms of the probabilities this means that the amplitude is larger on the right side. So the particle position is more probable on the side where the potential barrier is larger. It is obvious that the nodes are more dense on the left when the potential is present, but even after the potential influence is passed, the behaviour continues so that the right side becomes wider. We can check this result also from the probabilities of the case $k = 4$ and $L = 5$. Let us examine a similar area symmetrically for the seventh energy eigenstate E_7. On the left we examine $0 \leq x \leq 2$ and on the right $3 \leq x \leq 5$. This gives us the probability on the left side

$$P^{E_7}_{0\leq x\leq 2} = 32.1\% \tag{63}$$

and on the right side

$$P^{E_7}_{3\leq x\leq 5} = 44.6\%. \tag{64}$$

The difference is actually quite large. If the functions were normal trigonometric functions as in the particle in a box, the probabilities would be the same. Let us see the same results for seventh energy eigenstate of the derivative boundary. On the left side we have

$$P^{E^D_7}_{0\leq x\leq 2} = 30.0\% \tag{65}$$

and on the right side

$$P^{E^D_7}_{3\leq x\leq 5} = 48.5\%. \tag{66}$$

Here the difference is even larger than for the normal boundary. This means that after the potential barrier has been passed the energy eigenstates behave so that the particle is more probably found on the right side of the box. As for in the beginning for the lowest energy eigenfunctions the situation is the opposite. They are more likely to be found on the left side.

Now let us choose a much larger potential curve. We choose $k = 10000$ and $L = 1$. There we can witness that the particle is actually more likely to be in the

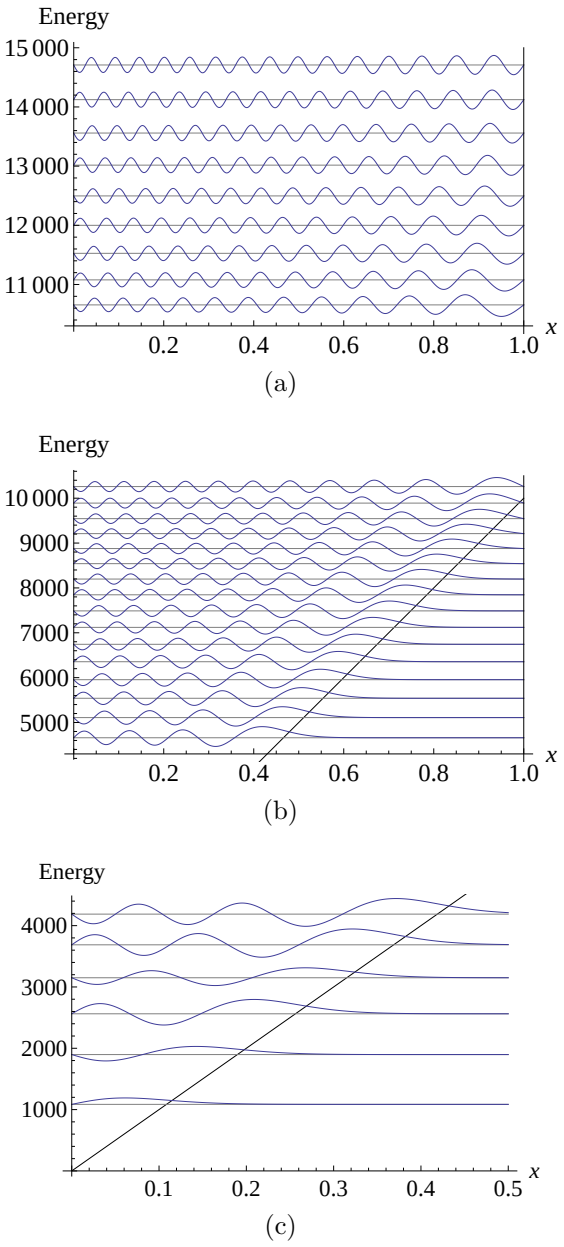

Figure 12: Energy eigenfunctions with the parameters $k = 10000$ and $L = 1$. (a) Energy values from 10 300 to 15 000. The quantum number $n \in [23, 30]$. (b) Energy values from 4300 to 10 200. The quantum number $n \in [7, 22]$. (c) Energy values from 0 to 4200. The quantum number $n \in [1, 6]$

vicinity of the potential curve and being on the classically forbidden area is very probable compared to the lower potential curve slopes. We have plotted this into a several figures so that it is easier to see the behaviour more precisely and it is shown in Figure 12. In the lowest case Figure 12c we have the starting points with the quantum number n going from 1 to 6. We can see clearly that the wave function can penetrate the classically forbidden area. It is also notable that the probability is again higher in the proximity of the potential barrier than the wall barrier on the left. In Figure 12b and Figure 12a we have continued to plot the wave functions corresponding to the quantum number n going from 7 all the way to 30. In the middle Figure 12b we see the behavior when we are facing the potential barrier on the right side. The figure is in the line with our previous work above. So the left side is more dense than the right side. In Figure 12a we enter the area outside of the potential barrier. For the first wave functions we can still see that the right side is much wider than the left. When the quantum number increases towards $n = 30$ it seems that the situation is again resembling more and more of the particle in the box case. But still it is notable that the right side is wider even though $n = 30$.

The fact that the probability amplitude of the wave function solutions are mostly concentrated next to the potential barrier is expectable. This phenomenon is called the turning point effect. It shows up very clearly in the semi-classical WKB-solutions. This is the point where the particle is to classically change its direction and turn back so it does not exist in the quantum world. It is therefore the slowest part of the whole process because the probability amplitude only sees the probability and it disregards the actual turning of the particle. There we can get that the most probable place to be is in the vicinity of the potential barrier which is also supported by the quantum theory. [27]

2.2.3 Comparison

First we want to compare our findings to the particle in a box. Before that we will present briefly the well-known solution for the particle in a box. It is not necessary to go into the actual calculations and we will just present the final result and the formulas with their proofs can be found in [27]. It is one of the basic calculations and it is found in almost every book that covers the basis of quantum mechanics. We just remind that this textbook example is solvable analytically, and usually the way to the solution is presented with two different approaches having the same outcome. It is one of the most referred results in all quantum mechanics. We wish to show that our chosen potentials start to behave like a particle in a box when the potential

is not present nearby. So either when the chosen potential parameter k is so gradual that it almost looks entirely like the particle in a box, or in the energy levels that are much higher than the level where the potential touches the wall.

We will denote the potential of the particle in a box by $V_B(x)$ where the subindex B refers to the box. The potential translated into mathematics is

$$V_B(x) = \begin{cases} 0, & 0 < x < L \\ \infty, & x \leq 0 \wedge x \geq L \end{cases} \tag{67}$$

where L is again the length of the box and x obviously denotes the position of the particle in the box. The normalized solution for the wave function is a trigonometric function and it is again important to note that the Schrödinger equation for this system can be solved analytically

$$\psi_{B,n} = \sqrt{\frac{2}{L}} \sin\left(\frac{n\pi}{L}x\right), \tag{68}$$

where B again denotes the box and n refers to the quantum number of the energy eigenstate. It is notable that n is a positive integer

$$n \in \{1, 2, 3, 4, \dots\}. \tag{69}$$

Now we have solution but there are quite a few properties that can be easily shown to exist for this system.

If the box length is L, the wavenumber k_n is

$$k_n = \frac{n\pi}{L} \tag{70}$$

where n is the quantum number. It is important to notice that the wavenumber k_n has nothing to do with our potential parameter k. They both are chosen for historical purposes and it is important to see that they are completely different parameters. From these we will get a simple formula for the energy eigenvalues that we label $E_{B,n}$ according to our previous sub index system

$$E_{B,n} = \frac{\hbar^2 k_n^2}{2m}. \tag{71}$$

Now that we substitute (70) into (71), we will get the energy eigenvalues for adjusting the length of the box L. Let us also recall that previously we made the assumption that the mass $m = 1/2$ and the Dirac constant $\hbar = 1$. This gives us the energy

eigenvalues of the box solution in an even more simple form

$$E_{B,n} = \frac{n^2\pi^2}{L^2}. \tag{72}$$

From this we will also make a remark that under our assumptions the energy eigenvalue $E_{B,n}$ from (72) is actually the square of the wavenumber k_n. One of the properties of the particle in a box solution is that the energy eigenvalues are tied to the lowest energy value which can be easily seen from (72). The relations of the energy values are proportional to the square of the energy state number n as

$$\frac{E_{B,n}}{E_{B,1}} = n^2. \tag{73}$$

This is also one of the things we will compare to the energy eigenvalues of the linear potential in an infinite well.

First we compare the particle in a box with the linear potential with the parameters $k = 1$ and $L = 1$. The results are in the Table 1. For clarity we have denoted the energy of the linear potential solution as a function of the potential parameter $E_n(k)$. In this way it is easier to show the actual situation of the parameters in the table. In the table you will find that the energy eigenvalues differ from each other approximately 0.5 energy units so they are very close and consistent. The energy proportions are also quite close. The larger the energy, the larger the difference. This is of course obvious and expected because of the relation being proportional to the square of the state number n. This case is found to be quite similar to the situation of the mere particle in a box.

The comparison of the case $k = 50$, $L = 1$ is made in Table 2. There we can see that the lowest energies are completely different. This makes the energy relation to the lowest energy useless to compare as can be seen in the table. For this reason we will not present the energy relation comparison again for the higher potential parameters. When we get close to the 12th energy state, the energies are starting to look quite similar. So even though the barrier is still quite small and only the lowest energy state collides with the barrier, the energy eigenvalues differ drastically from the particle in a box. But when the quantum number n goes high enough, the energies of the two different potential cases start to once again resemble one another, as it was expected.

Now we will present a nice illustration of the comparison between the cases. In Figure 13 we can see the behavior of the ratios of the energy eigenvalues compared to

n	$E_n(k=1)$	$E_{B,n}$	$E_n(k=1)/E_1(k=1)$	n^2
1	10.3685	9.8696	1	1
2	39.9787	39.4784	3.85579	4
3	89.3266	88.8264	8.61519	9
4	158.414	157.914	15.2784	16
5	247.240	246.740	23.8453	25
6	355.806	355.306	34.3160	36
7	484.111	483.611	46.6905	49
8	632.155	631.655	60.9687	64
9	799.938	799.438	77.1507	81
10	987.460	986.960	95.2365	100
11	1194.72	1194.22	115.226	121
12	1421.72	1421.22	137.119	144
13	1668.46	1667.96	160.916	169
14	1934.94	1934.44	186.617	196

Table 1: $k = 1$, $L = 1$. $E_n(k = 1)$ is the energy eigenvalue of the linear potential case for each n. $E_{B,n}$ refers to the particle in a box.

n	$E_n(k=50)$	$E_{B,n}$	$E_n(k=50)/E_1(k=50)$	n^2
1	32.2505	9.8696	1	1
2	65.177	39.4784	2.02096	4
3	114.309	88.8264	3.54442	9
4	183.212	157.914	5.6809	16
5	271.938	246.74	8.43207	25
6	380.446	355.306	11.7966	36
7	508.715	483.611	15.7739	49
8	656.735	631.655	20.3636	64
9	824.502	799.438	25.5656	81
10	1012.01	986.96	31.3797	100
11	1219.27	1194.22	37.8061	121
12	1446.26	1421.22	44.8446	144
13	1692.99	1667.96	52.4951	169
14	1959.47	1934.44	60.7578	196

Table 2: $k = 50$, $L = 1$. $E_n(k = 50)$ is the energy eigenvalue of the linear potential case for each n. $E_{B,n}$ refers to the particle in a box.

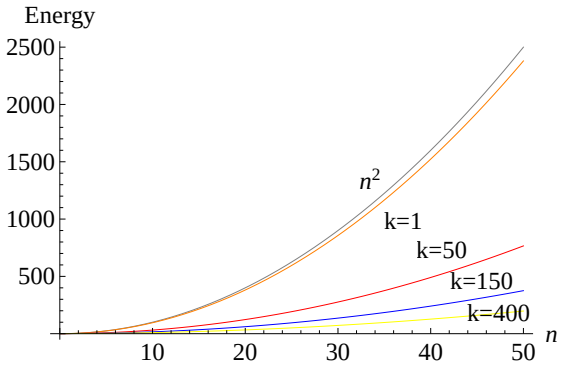

Figure 13: Comparison with the different solutions of the parameter k to the particle in a box situation n^2.

the lowest energy eigenvalue in both the particle in a box and in the linear potential. The particle in a box situation is illustrated as the function n^2 since it behaves as the square of the quantum number n. Now as expected the situation when $k = 1$ behaves very much like the particle in a box. This ratio is plotted with an orange color. The plots were made with Mathematica by fitting a function to the calculated ratios by the least-square method. With the Mathematica commands we refer to [28]. As the potential slope k increases, the results vary more the mere box. This is of course logical that when more and more potential is present, we will start to lose the results given by the simple box model. The case $k = 10000$ is so far from the n^2 that there is no point in plotting it into this figure.

The increase of the parameter k causes the ratio to get smaller. This means that the first energy eigenvalue is experiencing the potential already at such a high energy rate that it will twist the ratio calculation. This can be seen in the tables we presented earlier. The really interesting fact in this is that even though the results go further from the box, the resulting functions are still in the form of n^2. The functions just get some constant a in front of them but the behavior is in the power of a n^2-function. The actual functions in our study are presented in Table 3. There we can see that the $k = 10000$ situation is far beyond from the other four when we are looking at the n^2-behavior. The potential there is already so large that it is not anymore reasonable to compare the ratio. But other than that, we get quite nice results with the n^2-approach. The behavior of the $k = 10000$ is still so interesting that we seek to find its corresponding fit. This is why the n^3-behavior is also added to the Table 3. The n^3 behavior obviously has nothing to do with the original idea of the particle in a box but it is interesting to find out that the fit actually resembles the n^3 to a very great taste.

k	$a + cn^2$	$a + bn + cn^2 + dn^3$
1	$0.048 + 0.952n^2$	$0.048 + 5.758 \cdot 10^{-5}n + 0.952n^2 + 3.054 \cdot 10^{-7}n^3$
50	$0.771 + 0.306n^2$	$0.688 + 0.045n + 0.300n^2 + 2.365 \cdot 10^{-4}n^3$
150	$1.117 + 0.150n^2$	$0.804 + 0.168n + 0.127n^2 + 0.001n^3$
400	$1.508 + 0.079n^2$	$0.684 + 0.428n + 0.023n^2 + 0.002n^3$
10000	$4045 + 12.07n^2$	$461.0 + 749.5n - 24.64n^2 + 0.495n^3$

Table 3: The fitted functions for the values of the k. The first column tells the n^2 behavior with two independent parameters a and c. The second column tells the n^3 behavior with four independent parameters a, b, c and d.

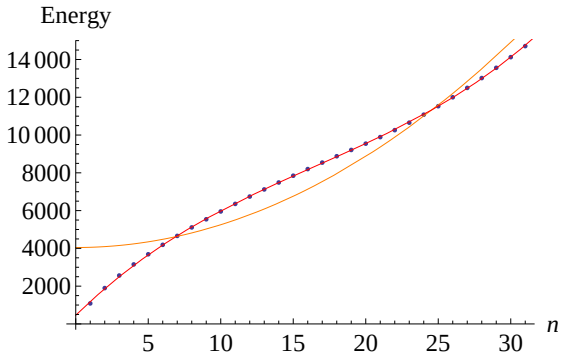

Figure 14: The Flügge fitted solution comparison when the parameter $k = 10000$. Blue dots are the calculated energy points, the orange line is the x^2-function and the red line is the x^3-function.

All in all in Table 3 we first notice that when $k = 1$, the parameter is close to zero as it is in the box. The parameter c is close to one. As the k goes larger the a parameter grows because function is differing from the zero point. At the same time the c parameter decreases which causes the actual function to spread wider. The case $k = 10000$ is inconsistent with these findings because the energy of the first eigenstate is so different from the box case. Again in comparing to the n^3 function we will see that with the small values of k, we are close to the n^2 solution. That means that the parameters b and d are close to being zero. We have plotted the $k = 10000$ situation separately to state that the n^2 and n^3 fits are very different. In Figure 14 we have plotted this so that the dots represent the actual measurement points in the calculation, the orange line is the n^2 function and the red line is the n^3 function. We can see that the n^2 solution does not give even a close fit, as the n^3 is extremely precise. It is also important to note that the n^3 solution needs all of its four free parameters to get this close result.

The other major comparison we want to address is the study of S. Flügge where

one of the problems in his book is the free fall of a body over earth's surface.[12] The idea in the problem presented is that there is a particle moving in a homogeneous gravity field over the surface of the earth. Basically the potential is as in our study expect that the right handed side infinite wall is missing. The potential $V_F(x)$, where the F stands for Flügge, is

$$V_F(x) = \begin{cases} mgx & x > 0 \\ \infty & x \leq 0 \end{cases} \tag{74}$$

where m is the particle mass and g is the gravitational acceleration. This will also end up to solutions that are in the form of the Airy functions. But we do not go deeper into that solution. Our interest here lies within the energy eigenvalues E_n. After some calculations and estimates, we end up having a formula for the energy eigenvalues. This is valid for only when the quantum number $n \gg 1$. All in all in our study the comparison between the Flügge solution is reasonable in the case of $k = 10000$. There we have over twenty wave functions that experience the linear potential. So especially those that are not close to the ending part of the linear potential in the right-hand side, are experiencing the potential as there were no infinite wall on the right side at all. This should look like the Flügge solution. Now we have the approximated energy from Flügge when $n \gg 1$

$$E_{n,F} = \frac{\hbar^2}{2ml^2}\left(\frac{3\pi}{4}\left(2n - \frac{1}{2}\right)\right)^{\frac{2}{3}}. \tag{75}$$

Here the parameter l stands for the characteristic length of the system. Basically what we have here is a dependence of the quantum number n and some constant C. We want to find out that can we find some constant in our solutions especially regarding the case $k = 10000$ when $n \in [1, 23]$, that is when there is a linear potential present. We are interested about the ratio of our previously defined energies and their corresponding quantum numbers. If that is a constant, then we have a resemblance to the Flügge solution, which is expected. Then it gives us satisfaction that the solutions are similar in a way. We will proceed with dividing our energy eigenvalues with the factor

$$\left(2n - \frac{1}{2}\right)^{\frac{2}{3}} \tag{76}$$

and see if we end up with a constant. The result for the case $k = 10000$ is plotted

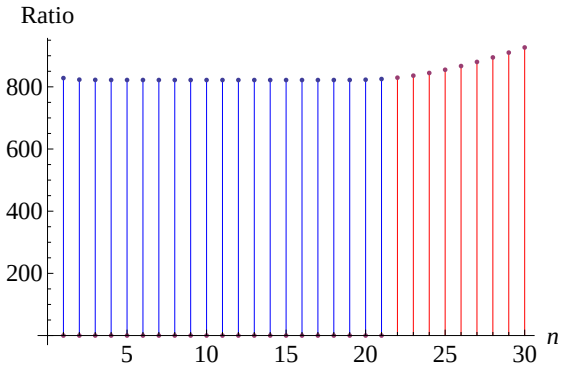

Figure 15: Comparison to the Flügge solution when $k = 10000$. Blue refers to the linear potential impact area and the red values are n values above that.

in Figure 15. It is shown that the ratio in fact stays a constant even though of the restriction of $n \gg 1$ in (75). We see some variation in the beginning just as can be expected from the n value restriction. Also when the n closes at the end of the linear potential, the values start to increase a bit. When the values do increase the linear potential, the ratio is no longer a constant and it is rising in a fast manner. The quantum states not colliding with the linear function are plotted with red color. These are the values $n \in [22, 30]$. This tells us that our solution is in sync with the Flügge solution.

We also wanted to take the case $k = 400$ into the comparison just for the idea of the whole thing. It actually works pretty well for that case too. At least when the wave functions face the linear potential. This happens when $n \in [1, 4]$. The ratio calculated by dividing with (76) gives good results for the first four quantum numbers n. The first one also is a bit distracted but this is due to the restriction mentioned earlier. This is shown in Figure 16. Again the quantum states colliding the linear potential are blue and the states above those are red in color. From here we can also see that the values start to increase immediately when turned to the red zone. This again reassures us about the similarity of our solution and the Flügge solution, when we are dealing with the area of the linear potential.

Finally we want to demonstrate the Flügge energy formula (76) in the manner we did in Table 3. There we were seeking how to fit the calculated energy points to the energy ratio. We used an n^2 model based on the particle in a box solution and a four parameter n^3 model just to find a proper fit to the $k = 10000$ case. We can also do the fit using only one parameter and the Flügge energy formula (76). This is interesting only for the $k = 10000$ case so we focus only on it. The actual fitted

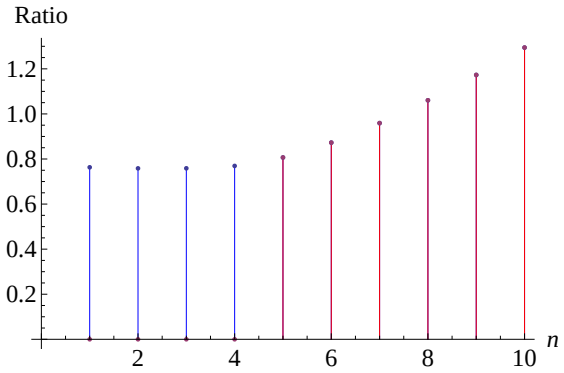

Figure 16: Comparison to the Flügge solution when $k = 400$. Blue refers to the linear potential impact area and the red values are n values above that.

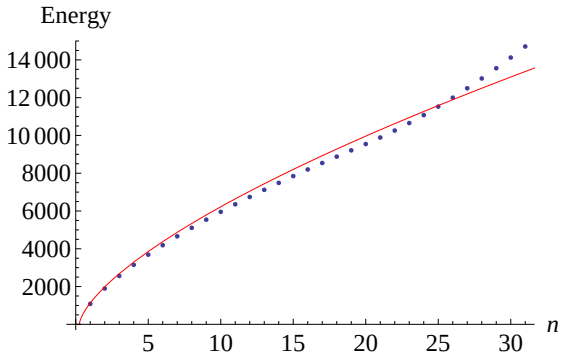

Figure 17: Comparison to the Flügge solution when $k = 10000$. Blue dots are the calculated energy points and the red line is the fitted function (77).

function is

$$859.047 \cdot \left(2n - \frac{1}{2}\right)^{\frac{2}{3}}. \tag{77}$$

In Figure 17 we can see how this fits with the calculated energy points. The result begins to differ starting from $n = 26$. From there on the potential is no longer the linear potential but the infinite wall barrier thus making the Flügge solution incompatible. The actual energies outside the linear potential start from $n = 22$ but the fit is made from all the energy values so it stays on a bit longer.

2.2.4 Summary

Our starting point was that we have a physical experiment which has a 3-dimensional magnetic field that is our potential. We simplify this situation to a 1-dimensional

case. Now we have obtained the solution for the linear potential in an infinite well by using numerical methods. The solution is a sum of two Airy functions and it is dependent of the potential parameter k and the length of the well L. Two different solutions are made according to the two different boundary conditions. The normal boundary conditions (44) and the derivative boundary conditions (45). The analysis of the solution is done for a handful of different parameter values. The main thing is to notice that the solutions with the normal boundary behave similarly to the particle in a box situation, when the potential slope k is small. When the slope is larger, the energy eigenfunctions above the potential start to resemble the particle in a box situation. Their behavior is scaled on higher energies due to the impact of the potential barrier. This was expected beforehand and now we have the results from our calculations.

The behavior of the derivative boundary case is also quite similar. The most important notice there is that the first energy eigenfunction does not have zero points. Starting from the second state we will start to have one zero point, on third state we have two zero points and so on.

The probabilities of the lowest energy eigenstates are concentrated on the left on smaller values of k. There also exists a small probability that the particle can be found from the other side of the barrier, which is the classically forbidden area. When the parameter k becomes larger and especially with the eigenstates above the barrier, we will start to see that the probability is larger on right side. This makes a difference with the particle in a box situation. In box solution the probabilities are the same on both the left and the right side due to the trigonometric behavior.

The really interesting part comes when we start to compare our results with the Flügge solutions. In the Flügge situation we have the linear potential with an infinite wall only on the left side. We obtain that our results resemble the Flügge solution with very great accuracy when the potential parameter k is large and the energy eigenstates are colliding with the potential barrier. Especially Figure 15 shows this extraordinary well. The resulting ratio starts to differ from the constant of the Flügge solution immediately after the energy eigenfunctions are no longer colliding with the potential barrier.

3 Infinite well with an inverted oscillator potential

3.1 Parabolic cylinder functions

In this section we look into one dimensional system in an infinite well with an inverted oscillator potential

$$V(x) = -\frac{1}{2}kx^2, \tag{78}$$

when $x \in [-L, L]$. L is the length of the well. We will solve the energy eigenvalues and eigenfunctions using an approximation method. The solutions for this type of differential equation are parabolic cylinder functions. Again we refer to [23] with the special functions.

Basics about the parabolic cylinder functions lead way back to the 19th century and the studies of the German physicist Heinrich Friedrich Weber. He is not to be confused with a contemporary mathematician Heinrich Martin Weber who was actually born a year before and died a year later than H.F. Weber. H.F. Weber was actually the first doctoral thesis supervisor for Albert Einstein. They did not get along very well and eventually Einstein changed to a different supervisor.[29]

The parabolic cylinder functions are actually sometimes even named Weber functions. In some sources the solution is given by some other class of special functions which are related to the parabolic cylinder functions via specific transformations. The standard solution is given with the parabolic cylinder function $D_a(x)$. The differential equation in its full form is

$$y''(x) + (ax^2 + bx + c)y(x) = 0. \tag{79}$$

The differential equation has a special property regarding its solutions. If one of these

$$y(a, x) \qquad y(a, -x) \qquad y(-a, ix) \qquad y(-a, -ix) \tag{80}$$

is a solution, they all are solutions. The equation (79) can be divided into two real equations that are independent. We will first rewrite the equation (79) by

completing the square and get

$$y''(x) + \left[a\left(x + \frac{b}{2a} \right)^2 - \frac{b^2}{4a} + c \right] y(x) = 0. \tag{81}$$

Now we define a new variable α,

$$\alpha \equiv x + \frac{b}{2a}. \tag{82}$$

Obviously this also means that $d\alpha = dx$ because a and b are just mere parameters. We also define a new parameter d,

$$d \equiv \frac{b^2}{4a} + c. \tag{83}$$

By inserting (82) and (83) to (81), we end up having the equation

$$y''(\alpha) + (a\alpha^2 + d)y(\alpha) = 0. \tag{84}$$

For this we get two distinct forms

$$y''(x) - \left(\frac{1}{4}x^2 + a \right) y(x) = 0 \tag{85}$$

$$y''(x) + \left(\frac{1}{4}x^2 - a \right) y(x) = 0 \tag{86}$$

which are also called the Weber equations.[30] If you make replacements $a \to -ia$ and $x \to xe^{\frac{1}{4}i\pi}$, you will get (86) from (85).

In Figure 18 we can see a few different parabolic cylinder functions so that we can observe how it behaves. We will now focus on the latter of the two equations (86) because it is used in this text later. The solution can be given with an even and odd functions and it can take many different forms.

The solution can be given with power series. This is a very basic technique. We will have two solutions, for the even and the odd,

$$\begin{aligned} y_1(x) &= 1 + a\frac{x^2}{2!} + \left(a^2 - \frac{1}{2} \right) \frac{x^4}{4!} \\ &+ \left(a^3 - \frac{7}{2}a \right) \frac{x^6}{6!} + \left(a^4 - 11a^2 + \frac{15}{4} \right) \frac{x^8}{8!} + \dots \end{aligned} \tag{87}$$

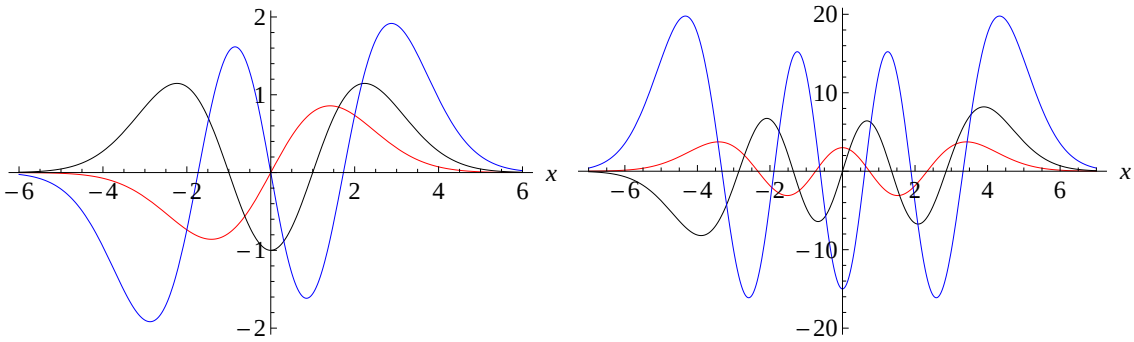

(a) (b)

Figure 18: Parabolic cylinder function $D_\nu(x)$. (a) The red curve is $D_1(x)$, the black curve is $D_2(x)$ and the blue curve is $D_3(x)$. (b) The red curve is $D_4(x)$, the black curve is $D_5(x)$ and the blue curve is $D_6(x)$.

and

$$\begin{aligned} y_2(x) &= x + a\frac{x^3}{3!} + \left(a^2 - \frac{3}{2}\right)\frac{x^5}{5!} \\ &+ \left(a^3 - \frac{13}{2}a\right)\frac{x^7}{7!} + \left(a^4 - 17a^2 + \frac{63}{4}\right)\frac{x^9}{9!} + \ldots \end{aligned} \tag{88}$$

Here we have a connection between a_n and $\frac{x^n}{n!}$. It is as follows

$$a_{n+2} = aa_n - \frac{1}{4}n(n-1)a_{n-2}. \tag{89}$$

The functions y_1 and y_2 can also be given with the Kummer function

$$M(a,b,z) = {}_1F_1(a;b;z) \tag{90}$$

$$= \sum_{n=0}^{\infty} \frac{a^{(n)}z^n}{b^{(n)}n!}, \tag{91}$$

where the symbol $a^{(n)}$ is

$$a^{(0)} = 1 \tag{92}$$

$$a^{(n)} = a(a+1)(a+2)\cdots(a+n-1). \tag{93}$$

The Kummer functions belongs to the group of the confluent hypergeometric functions. The function is named after Ernst Kummer who was a German mathematician

in the 19th century.[31] We have for y_1 that

$$y_1 = e^{-\frac{1}{4}x^2} M\left(-\frac{1}{2}ia + \frac{1}{4}, \frac{1}{2}, \frac{i}{2}x^2\right) \tag{94}$$

$$= e^{-\frac{1}{4}x^2} {}_1F_1\left(-\frac{1}{2}ia + \frac{1}{4}; \frac{1}{2}; \frac{i}{2}x^2\right) \tag{95}$$

and for y_2

$$y_2 = xe^{-\frac{1}{4}x^2} M\left(-\frac{1}{2}ia + \frac{3}{4}, \frac{3}{2}, \frac{i}{2}x^2\right) \tag{96}$$

$$= xe^{-\frac{1}{4}x^2} {}_1F_1\left(-\frac{1}{2}ia + \frac{3}{4}; \frac{3}{2}; \frac{i}{2}x^2\right). \tag{97}$$

The equations have complex numbers but the imaginary part identically vanishes after the sum is done. The standard solution for the equation (86) can also be given with the function $W(a, \pm x)$ and it is

$$W(a, \pm x) = 2^{-\frac{3}{4}} \left(\sqrt{\frac{G_1}{G_3}} y_1 \mp \sqrt{\frac{2G_3}{G_1}} y_2\right) \tag{98}$$

$$= \frac{[\cosh(\pi a)]^{\frac{1}{4}}}{2\sqrt{\pi}} (G_1 y_1 \mp \sqrt{2} G_3 y2), \tag{99}$$

where G_i is a Gamma function

$$G_1 = \left|\Gamma\left(\frac{1}{4} + \frac{1}{2}ia\right)\right| \tag{100}$$

$$G_3 = \left|\Gamma\left(\frac{3}{4} + \frac{1}{2}ia\right)\right|. \tag{101}$$

As a comparison of the study in Chapter 2, we present the parabolic cylinder function in terms of the Bessel function. Again we will only concentrate on the equation (86). With the Airy functions we have that they are Bessel functions of order $\frac{1}{3}$. The parabolic cylinder functions are Bessel functions of order $\frac{1}{4}$ and $\frac{3}{4}$

$$J_{\pm\frac{1}{4}}\left(\frac{1}{4}x^2\right) = \frac{2^{\frac{1}{4}}}{\sqrt{\pi x}} \left(W(0, -x) \mp W(0, x)\right) \tag{102}$$

$$J_{\pm\frac{3}{4}}\left(\frac{1}{4}x^2\right) = \frac{-2^{\frac{1}{4}}}{x\sqrt{\pi x}} \left(W(0, x) \pm W(0, x)\right). \tag{103}$$

Even though they seem a bit complicated we can see that the different special

functions have a lot of connections with each other.

3.2 Solutions

3.2.1 Solving the Schrödinger equation

The harmonic oscillator is one of the most profounding examples of all physics. In quantum mechanics the harmonic oscillator problem is a well-known textbook example like the particle in a box. It too can be solved analytically in an elegant way and the solution is a Hermite polynomial corresponding a specific energy eigenstate.[27] Our interest lies when we invert the harmonic behavior and trap it in an infinite well. Thus we get the inverted harmonic oscillator in an infinite well. This has also been studied in [32] and [33] to which we also refer in the procedure of this section. There are also reports with the ordinary harmonic oscillator in an infinite well [34], [35], [36], [37], [39] and [40].

The inverted harmonic oscillator in an infinite well also resembles the double-well potential which is quite similar. It too has a potential maximum in the center of the system and infinite walls on the edges. The double-well is obviously more round and does not have any discrete changes in the system. In our case we have sharp edges when going from the inverted oscillator to the walls. It is also notable that the walls are not straight upwards in the double-well like they are in our system. The double-well is also studied in an infinite well [41].

The corresponding Schrödinger equation for the inverted oscillator in an infinite well is

$$-\frac{\hbar^2}{2m}\psi''(x) - \frac{1}{2}kx^2\psi(x) = E\psi(x), \tag{104}$$

when $x \in \{-L, L\}$ and zero elsewhere. The parameters and terms represent the same as in (43), that is the Planck constant $\hbar$, mass m, wave function ψ, potential parameter k, position x and the corresponding energy E. First we substitute the following to the equation (104)

$$t = (4km/\hbar^2)^{1/4}x \tag{105}$$

$$a = -\frac{E}{\hbar\omega}, \tag{106}$$

where $\omega = \sqrt{\frac{k}{m}}$. The variable t is not to be confused with time. As it can be seen from (105) that it is just a scaling for the original position variable x. Now we have

the Schrödinger equation (104) for our system in the form

$$\frac{d^2y(t)}{dt^2} + \left(\frac{1}{4}t^2 - a\right) y(t) = 0, \tag{107}$$

which is the Weber equation (86) for the parabolic cylinder function. This has a solution

$$y(t) = Ay_1(t) + By_2(t), \tag{108}$$

where $y_1(t)$ is the even and $y_2(t)$ the odd function. They can be written as [32]

$$y_1(t) = 1 + \sum_{n=1}^{\infty} \frac{t^{2n}}{(2n)!} c_{2n} \tag{109}$$

$$y_2(t) = t + \sum_{n=1}^{\infty} \frac{t^{2n+1}}{(2n+1)!} c_{2n+1}, \tag{110}$$

where we have a recursion

$$\begin{cases} c_0 = c_1 = 1 \\ c_{-1} = c_{-2} = 0 \\ c_n = ac_{n-2} - \frac{1}{4}(n-2)(n-3)c_{n-4}. \end{cases} \tag{111}$$

Our boundary conditions from the potential barrier are

$$\psi(-L) = \psi(L) = 0 \tag{112}$$

which means that combining this with the substitution from equation (105) we get that

$$y\left(\left(\frac{4km}{\hbar^2}\right)^{1/4} L\right) = y\left(-\left(\frac{4km}{\hbar^2}\right)^{1/4} L\right) = 0. \tag{113}$$

We label this

$$L_0 = \left(\frac{4km}{\hbar^2}\right)^{1/4} L. \tag{114}$$

From the function parity we will gain that we must have either

$$\begin{cases} y_1(L_0) = 0 \\ B = 0 \end{cases} \tag{115}$$

or

$$\begin{cases} y_2(L_0) = 0 \\ A = 0 \end{cases} \tag{116}$$

which tells us that our even and odd solutions in (109) and (110) can be treated and solved separately from each other. It is important to note that now we have the energy E and the dimensionless energy quantity a, and they have opposite signs. In the end when we plot the energy eigenfunctions and show the eigenvalues, we will show them with the sign corresponding to E because it is physically more logical and by doing that it is easier to notice the actual results from the figures.

The details of the solution are presented in the Appendix B. We solve the equations (110) and (109) with the boundary conditions by taking a certain fixed number N of the polynomials. Each root of the equations y_1 and y_2 gives an energy eigenvalue a. We just simply need to discard the imaginary solutions, and by taking the real solutions in order we finally get our energy values. From the energy eigenvalues we can solve our energy eigenfunctions by normalizing the wave function. We have several figures that demonstrate this and we will next go on to the illustrations of our solutions.

3.2.2 Analysis

The analysis will start by simply plotting the solutions. We divide this into three cases that are small, medium and large box. It is to be noted that the box size and the potential parameter are linked in our substitutions. Unlike in Chapter 2 we only have one parameter to adjust. That is the width of the well, L. The full width of the well in this case is of course $2L$ due to the restriction that $x \in [-L, L]$. Our substitution (105) takes away the potential parameter k that causes the loss of one parameter. This is not a problem, on the contrary. Our Schrödinger equation is of the form

$$\frac{d^2y(t)}{dt^2} + \left(\frac{1}{4}t^2 - a\right) y(t) = 0, \tag{117}$$

where we can see that our actual potential is

$$V(t) = \frac{1}{4}t^2. \tag{118}$$

The equation (118) tells us our potential and the box length L specifies how large the actual potential is. When you make the length L larger, the potential grows wider at the same time. So only by scaling the box we can adjust the potential. It is also noticeable that due to our choices we have the values so that the inverted harmonic oscillator potential is below the energy zero point. This makes it easy to compare the energies and we can immediately see which energy eigenvalue is in the impact area of the potential and which are not simply by looking at their sign. The negative energy eigenvalues E are on the impact area and have the possibility to be in the classically forbidden area of the potential, the positive energy eigenvalues on the other hand only face the walls on the sides of the well.

One key factor is also the polynomial factor N. The number N is a fixed number used for the wave function's series in (109) and (110). This factor tells us how accurate our approximation is. In this analysis, when we present the figures, we have used $N = 22$. We will do a comparison on different values of N in the following subsection so that we can see how they behave and how accurate they are. The larger the box, the more we start to lose our accuracy. It is also worthy of mentioning that the calculations and especially the function illustrations take a lot of computer power. The figures presented here take time from several minutes to hours.

Let us begin our analysis with the small box. The length of the small box is $L = \frac{\sqrt{2}}{4}$ which is chosen by historical reason followed by [32]. The potential in this case is also very small and the system resembles quite a lot of the particle in a box solution which we already discussed in the previous chapter. There are no energy eigenfunctions in the impact area of the potential function. We can see the results from Figure 19. We have only the potential in Figure (19b). This is below the energy zero point and we can only see the potential because there are no energy eigenfunctions there. Figure (19a) shows the system above the energy zero point. It is actually plotted that the energy $E \in [-1, 170]$ so in theory it would be possible to see the inverted oscillator potential. This again proves how small the potential area is in this case. The actual energy eigenfunctions behave in a very similar manner as with the particle in a box case. You can see the expected trigonometric-like behavior. The blue line is the even function from (109) and the red line is the odd function from (110). We have the polynomial factor at our lowest and it is $N = 19$.

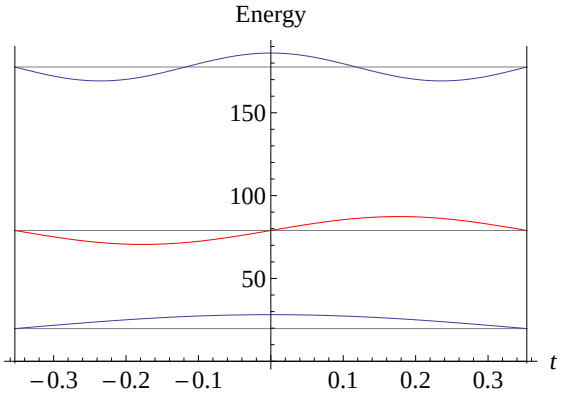

(a)

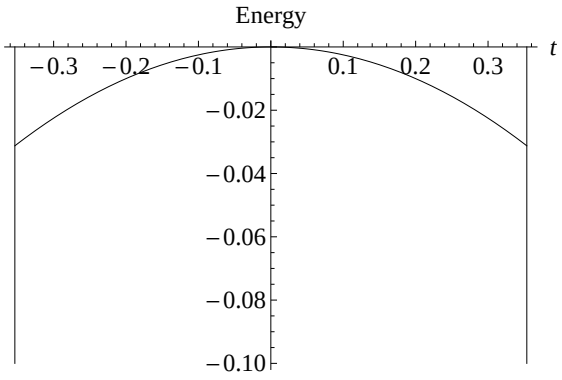

(b)

Figure 19: Small box length $L = \frac{\sqrt{2}}{4}$, the polynomial factor $N = 19$. The even energy eigenfunctions are blue, the odd energy eigenfunctions are red. The potential is black. (a) Energy eigenfunctions above the energy zero point. (b) No energy eigenfunctions below the energy zero point.

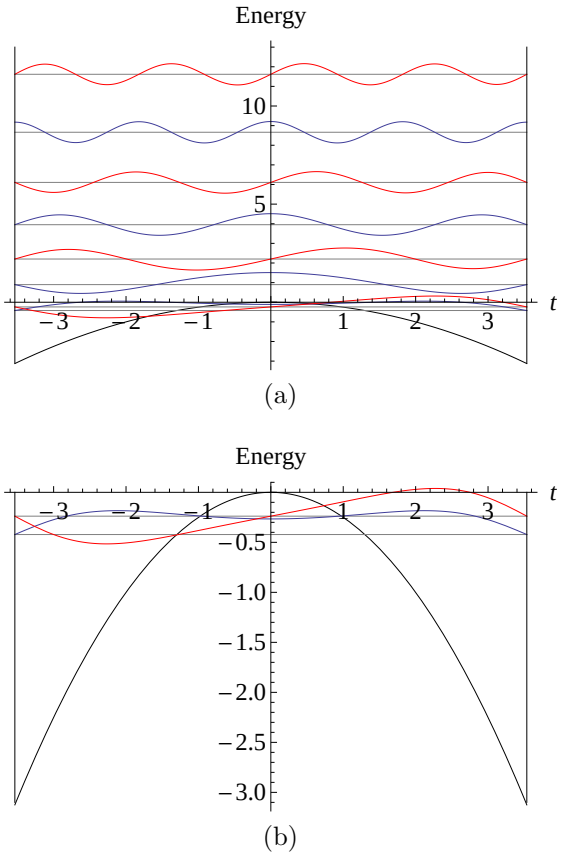

Figure 20: Medium box length $L = \frac{5\sqrt{2}}{2}$, the polynomial factor $N = 22$. The even energy eigenfunctions are blue, the odd energy eigenfunctions are red. The potential is black. (a) The energy eigenfunctions above and below the energy zero point. (b) A closer zoom to the potential of the medium box. Two energy eigenfunctions below the energy zero point.

The numerical part is not so heavy with this case so we can use a smaller polynomial factor and still get good results. The higher we take the factor N, the longer our computing lasts. Some scaling is also done in this analysis. In the case of the small box our scaling factor for the functions is 5. This is done only to ensure that the figures are large enough that we can see the behavior better.

Next we have the case of the medium box. Our box length is $L = \frac{5\sqrt{2}}{2}$. The results are plotted in Figure 20. Again the lower Figure 20b shows us the area below the energy zero point. In this case we can find two energy eigenfunctions in the potential impact area. It can clearly be seen that they have the possibility to be in the classically forbidden area. As it is predictable that they are more probable to be on the edges than in the center of the potential. Figure (20a) shows us the eigenfunctions above the energy zero point. There we can see that it starts to resemble the particle in a box almost immediately. We can calculate probabilities

for the particle being in the forbidden area for the first energy eigenstate a_1

$$P^{a_1}_{-0.6\leq x\leq 0.6} = 12.3\%. \tag{119}$$

There exists almost a 1/8-probability for the particle being in the classically forbidden area. We will check the probability for the second energy eigenstate a_2

$$P^{a_1}_{-1.8\leq x\leq 0.8} = 17.2\%. \tag{120}$$

This is even a bit larger than (119). It is important to notice that due to the scaling the values of t in the probability calculations differ from what can be seen from Figure 20b. The probabilities have been calculated without the scaling factors because they are used only to make the images larger. In Figure 20a there is no scaling but in Figure 20b it is 0.5. The polynomial factor is now $N = 22$ in order to have accurate energy eigenvalues and proper images. It is increased by 3 polynomial parts compared to the small box.

The last case is the large box, where the length is $L = 5\sqrt{2}$. It can be seen in Figure 21. Here the potential is scaled so that it starts to be so large that it really affects the system. In the lower Figure 21b we can see that there are already eight eigenvalues that are in the below energy zero point area. They are again concentrated on the edges of the system as it should but we can see that there are areas just next to the inverted potential where the particle can enter the classically forbidden range. One very interesting part in here is that the even and odd energy levels are extremely paired. This is also assumable from the double-well potential studies made in [13] and [41].

In the upper Figure 21a we can see the behavior above the energy zero point with six energy eigenstates. This should start to resemble the particle in a box system if we compare it with the previous cases. However the potential in this case is so large that the particle in a box solution is far from this even above the energy zero point. The pairing property of the even and odd solution can still be seen. Figures going far beyond this show that the numerical accuracy is starting to fail us the higher we go with the energy eigenfunctions. Our mathematical approximation can no longer sustain the system and the functions start to approach infinities near the wall. In this case we are already using the polynomial factor $N = 32$ of the original series. The approximation does not seem to be powerful enough for larger box lengths of L. This can also be seen as the computer power required to compute these figures and calculations. The larger the box, the longer it takes to perform the necessary

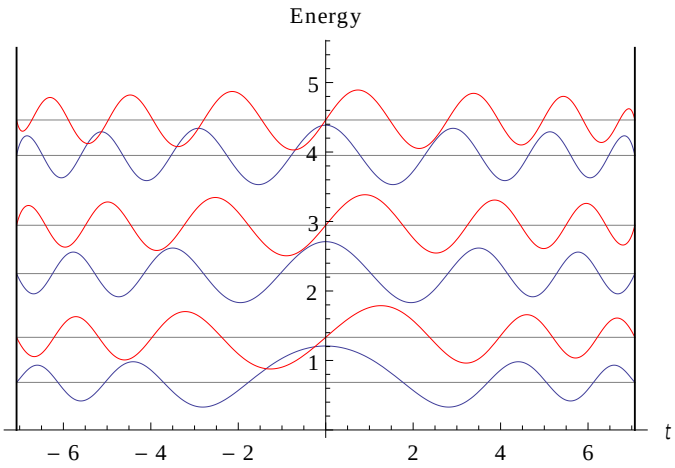

(a)

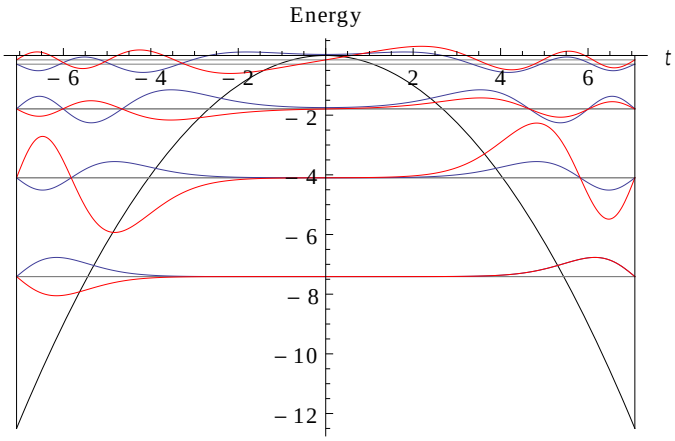

(b)

Figure 21: Large box length $L = 5\sqrt{2}$, the polynomial factor $N = 32$. The even energy eigenfunctions are blue, the odd energy eigenfunctions are red. The potential is black. (a) The energy eigenfunctions above the energy zero point. (b) The potential of the large box. Eight energy eigenfunctions below the energy zero point.

calculations and especially to plot the figures.

We can still see that the impact of the inverted harmonic oscillator potential does not exist anymore in the area above the energy zero point. The energy eigenfunction is more stable all over the box and there can no more be seen a classically forbidden area that that would make the energy eigenfunction go towards zero, as it did below the energy zero point. It is also worth to notice that the most probable place to be for the particle is still on the center of the system.

The numerical accuracy starts to play a role as we mentioned. The results can be twisted according the number N. The more we bring the polynomial factors, the more computer power our calculations need. This can be seen when we make the

box length wider. If we use the same polynomial factor N in the large box, we will have a result that the odd function is the first energy eigenstate. This is not coherent with the quantum theory and does not carry out the required equations. Next we will present some comparisons. First we will compare the energy eigenvalues from different polynomial factors N and also from the particle in a box solution.

3.2.3 Comparison

We will compare the results with the well-known particle in a box solution which has already been introduced in Chapter 2. The basic formulas and equations are in the previous chapter. The most important thing to remember is the energy ratio (73). It is the number divided by the first energy eigenvalue and it equals n^2.

First of we begin with the small box with the length of $L = \frac{\sqrt{2}}{4}$ and the results are in Table 4. The first energy column $E_{n,N=25}$ tells us the energy of the inverted oscillator case with a specific polynomial factor N at every quantum number n. The small box was so simple that it is only presented with one polynomial factor. The next energy column means the energy of the particle in a box situation and it is marked as $E_{n,box}$. Next we have the energy ratio of our system and after that the energy ratio of the particle in a box. As we look at the number in Table 4 we can very easily see that they are strikingly similar. Even at the largest quantum numbers like $n = 12$ we still have a great resemblance. This was also highly expected and can be seen from the Figure 19.

The medium box length is $L = \frac{5\sqrt{2}}{2}$ and the comparison is in the Table 5. Now we have three different polynomial factors N. They are similar with four digits to the $n = 10$. After that especially the $N = 19$ starts to differ but not that lot. When $n = 14$, the difference is the largest. The differences between the $N = 22$ and $N = 25$ start to affect when $n = 13$. That is why we choose to use the $N = 22$ in Figure 20 because in that analysis we only go to $n = 8$. Basically the $N = 19$ would also be sufficient but the $N = 22$ is a bit more accurate and it is a lot more economical to plot than $N = 25$. The energy eigenvalues of our case start from the negative side and the particle in a box is in the positive side. That is why the energies start to differ already from the beginning. But they are still quite close to each others. The energy ratios on the other hand have nothing in common.

The last case is the large box with the length $L = 5\sqrt{2}$ which can be seen in Table 6. Now the differences between the polynomial factors $N = 19$, $N = 22$ and $N = 32$ are large starting from the beginning. We can see that the data for $N = 19$ is something totally different but in a rough sense it is more or less gives results. It

n	$E_{n,N=25}$	$E_{n,box}$	$E_{n,N=25}/E_{1,N=25}$	n^2
1	19.73512	19.73920	1	1
2	78.94800	78.95684	4.00038	4
3	177.6432	177.6529	9.00137	9
4	315.8173	315.8273	16.0028	16
5	493.4701	493.4802	25.0047	25
6	710.6013	710.6112	36.0069	36
7	967.2109	967.2212	49.0096	49
8	1263.299	1263.309	64.0127	64
9	1598.866	1598.876	81.0162	81
10	1973.910	1973.921	100.020	100
11	2388.503	2388.444	121.028	121
12	2844.947	2842.446	144.157	144

Table 4: Small box length, $L = \frac{\sqrt{2}}{4}$.

has the pairing of the energy eigenvalues even though there are too many eigenvalues in the impact area of the potential. Same thing goes with the $N = 22$ but it is more subtle. Both of them have ten energy eigenstates below the energy zero point as for the $N = 32$ has eight and this makes a major difference. The other real problem with both the $N = 19$ and $N = 22$ is that the first energy state is odd which is not in line with the properties coming from solving the Schrödinger equation. In the case $N = 32$ we can see that the energy levels are extremely paired which explains why it almost seems that there are too few functions in the Figure 21. The real notable thing is that the energy levels are paired even after the potential impact area. This is interesting but it also happens with the double-well potential which is a case of resemblance in here. The comparison to the particle in a box becomes quite pointless because of the large amount of negative energies in the beginning. The ratio especially is absurd compared to the particle in a box.

We still want try to compare the results to the particle in a box. Rescaled comparisons are the thing we can more truthfully do the comparison. We rescale our system that our energy zero point starts from where the inverted oscillator hits the wall. It is obvious that the comparison to the box solution is not working because there are no negative energies in the box model. So the real comparison is between the absolute value of the first energy eigenstate and the compared ratio. If the first energy state is below zero and the latter are above it, the ratio is being distorted by the scaling. Adjusting the scaling may find us closer to the particle in a box situation. Even though it is likely of course that due to the inverted oscillator potential the first energy eigenstate is too different from the box model. This is

n	$E_{n,N=19}$	$E_{n,N=22}$	$E_{n,N=25}$	$E_{n,box}$	$E_{n,N=25}/E_{1,N=25}$	n^2
1	-0.422041	-0.422041	-0.422041	0.197362	1	1
2	- 0.238321	-0.238321	-0.238320	0.789568	0.564686	4
3	0.898556	0.898556	0.898556	1.776529	2.12907	9
4	2.202110	2.202110	2.202110	3.158273	5.21776	16
5	3.951576	3.951576	3.951576	4.934802	9.36301	25
6	6.106763	6.106763	6.106763	7.106115	14.4696	36
7	8.662547	8.662548	8.662549	9.672212	20.5254	49
8	11.61643	11.61644	11.61643	12.63309	27.5244	64
9	14.96727	14.96715	14.96715	15.98876	35.4637	81
10	18.71890	18.71399	18.71397	19.73921	44.3416	100
11	23.19091	22.85734	22.85647	23.88444	54.1569	121
12	25.85228	27.37060	27.39434	28.42446	64.9091	144
13	30.60393	31.09285	32.32152	33.35926	76.5838	169
14	31.53767	33.33248	37.86686	38.68885	89.7231	196

Table 5: Medium box length, $L = \frac{5\sqrt{2}}{2}$.

what happened when we were dealing with the linear potential in an infinite well in Chapter 2.

The rescaling is unnecessary for the small box case, where $L = \frac{\sqrt{2}}{4}$. There we have no negative energy eigenvalues of E_n and therefore it is fully comparable with the particle in a box as can be seen in the Table 4. The medium box can be scaled. The scaling is quite minor but still the negative energy eigenvalues distort the comparison otherwise. The scaling factor is obtainable with the simple procedure by adding the factor to the each separate energy eigenvalue from the box length L

$$\frac{\left(\frac{5\sqrt{2}}{2}\right)^2}{4} = \frac{25}{8}. \tag{121}$$

The results for the rescaled medium box are in the Table 7. We only took one polynomial factor $N = 25$ just to demonstrate the actual scaling procedure. We can see that the resemblance starts to be quite good. Especially the ratio is quite similar after we recalculated the particle in a box ratio using the rescaling.

In Table 8 we have the rescaled large box. We look at the largest polynomial factor $N = 32$. The energy values differ quite a lot especially in the beginning and in the end. In the mid areas they are not that far from each others. The ratio on the other hand is does not work closely at all. It works in the range for three numbers. After $n = 5$ we are starting to be quite far. It does not settle in the end also.

n	$E_{n,N=19}$	$E_{n,N=22}$	$E_{n,N=32}$	$E_{n,box}$	$E_{n,N=32}/E_{1,N=32}$	n^2
1	-8.997723	-7.552924	-7.41045	0.024674	1	1
2	-8.682850	-7.192064	-7.41027	0.098696	0.999976	4
3	-6.804082	-5.198092	-4.09957	0.222066	0.553215	9
4	-6.258838	-4.775125	-4.09834	0.394784	0.241917	16
5	-4.504370	-3.265979	-1.79271	0.616850	0.240800	25
6	-4.009475	-2.839196	-1.78443	0.888264	0.039246	36
7	-2.518685	-1.577325	-0.29083	1.209026	0.019829	49
8	-2.099986	-1.223216	-0.14694	1.579137	0.092356	64
9	-0.904717	-0.192373	0.68440	1.998595	0.179896	81
10	-0.624822	-0.120588	1.33311	2.467401	0.303663	100
11	0.271474	0.814645	2.25028	2.985555	0.397550	121
12	0.436659	1.130233	2.94603	3.553058	0.533169	144
13	1.531682	2.312187	3.95102	4.169908	0.602028	169
14	1.929939	2.735832	4.46130	4.836106	0.776510	196
15	3.309745	4.179993	5.75429	5.551652	0.837841	225
16	3.790054	4.669515	6.20878	6.316547	1.05559	256
17	5.467365	6.372688	7.82243	7.130789	1.12438	289
18	6.015212	6.920211	8.33216	7.994380	1.36999	324
19	8.008168	8.897799	10.1522	8.907318	1.44526	361
20	8.618252	9.499428	10.7100	9.869604	1.71693	400
21	10.97176	11.78420	12.7232	10.88124	1.79744	441
22	11.64156	12.43789	13.3199	11.94222	2.09761	484
23	14.43401	15.08323	15.5443	13.05255	2.18303	529
24	15.16281	15.78813	16.1773	14.21223	2.51502	576
25	18.53079	18.87925	18.6375	15.42126	2.60527	625
26	19.31949	19.63556	19.3062	16.67963	2.97345	676
27	23.53028	23.31680	22.0346	17.98735	3.06849	729
28	24.38214	24.12598	22.7389	19.34442	3.47892	784
29	30.12877	28.67705	25.7804	20.75084	3.57877	841
30	31.05236	29.54249	26.5203	22.20661	4.04015	900

Table 6: Large box length, $L = 5\sqrt{2}$.

n	$E_{n,N=25}$	$E_{n,box}$	$E_{n,N=25}/E_{1,N=25}$	$E_{n,box}/E_{1,box}$
1	2.70296	3.32239	1	1
2	2.88668	3.91457	1.06797	1.17824
3	4.02356	4.90153	1.48857	1.47530
4	5.32711	6.28327	1.97084	1.89119
5	7.07658	8.05980	2.61809	2.42590
6	9.23176	10.2311	3.41543	3.07944
7	11.7875	12.7972	4.36098	3.85181
8	14.7414	15.7581	5.45382	4.74299
9	18.0922	19.1138	6.69346	5.75301
10	21.8390	22.8642	8.07966	6.88185
11	25.9815	27.0094	9.61224	8.12952
12	30.5193	31.5495	11.2911	9.49601
13	35.4465	36.4843	13.1140	10.9813
14	40.9919	41.8138	15.1656	12.5855

Table 7: Rescaled medium box, length $L = \frac{5\sqrt{2}}{2}$.

3.2.4 Summary

We have investigated the properties of the inverted oscillator in an infinite well. The solutions are given by an approximation method that uses a certain long polynomial from the solutions (109) and (110) which we can decide using the factor N. One surprising element is that our initial changing of the variable causes that we have only one parameter. This removes totally the dependency of the potential parameter k which is very handy. The potential parameter is now tied with the length of the box L. As it is expected the cases resemble the particle in a box especially when the box length is small and after the potential does not make that large of an influence anymore. The large box starts to differ quite a lot from the particle in a box.

The solutions for the double-well potential implicate us that the even and odd solutions are paired. As expected we see the pairing especially well when the box size is large. We also see that if we have a strong harmonic potential, the pairing of energy eigenstates occurs even when we are not in the impact area of the potential. In the case of the large box we see that the energy levels are paired even though we go as up to the 30th energy eigenstate.

The numerical method works out quite well. It has its down sides also. It needs to be checked out that it really is giving the proper results. This can be done by using a higher polynomial factor N. When plotting the figures, the improper numerical functionality can be seen especially well. The figures approach infinities on near the edges of the wall and therefore the figure does not meet the requirements

of the original boundary conditions (113). These false figures are not shown in this work. All in all the method is very useful and convinient because it only uses a certain amount of the polynomial terms from which we get the solutions.

n	$E_{n,N=32}$	$E_{n,box}$	$E_{n,N=32}/E_{1,N=32}$	$E_{n,box}/E_{1,box}$
1	5.08955	12.5493	1	1
2	5.08973	12.6974	1.00003	1.0118
3	8.40043	12.9441	1.65053	1.03146
4	8.40166	13.2896	1.65077	1.05898
5	10.7073	13.7337	2.10378	1.09438
6	10.7156	14.2765	2.10541	1.13763
7	12.2092	14.9181	2.39887	1.18875
8	12.3531	15.6583	2.42714	1.24774
9	13.1844	16.4972	2.59049	1.31459
10	13.8331	17.4348	2.71794	1.38930
11	14.7503	18.4711	2.89815	1.47188
12	15.4460	19.6061	3.03485	1.56232
13	16.4510	20.8398	3.23231	1.66063
14	16.9613	22.1722	3.33257	1.76680
15	18.2543	23.6033	3.58662	1.88084
16	18.7088	25.1331	3.67592	2.00274
17	20.3224	26.7616	3.99297	2.13251
18	20.8322	28.4888	4.09312	2.27014
19	22.6522	30.3146	4.45073	2.41563
20	23.2100	32.2392	4.56033	2.56899
21	25.2232	34.2625	4.95589	2.73022
22	25.8199	36.3844	5.07312	2.89931
23	28.0443	38.6051	5.51017	3.07626
24	28.6773	40.9245	5.63454	3.26108
25	31.1375	43.3425	6.11792	3.45377
26	31.8062	45.8593	6.24931	3.65431
27	34.5346	48.4747	6.78540	3.86273
28	35.2389	51.1888	6.92377	4.07900
29	38.2804	54.0017	7.52137	4.30315
30	39.0203	56.9132	7.66674	4.53515

Table 8: Rescaled large box, length $L = 5\sqrt{2}$.

4 Tunneling

4.1 Introduction

4.1.1 About the history of tunneling theory

One of the major differences between classical and quantum worlds is the concept of tunneling. Quantum tunneling basically means that a particle can pass a potential barrier without having the sufficient energy to cross the barrier classically. A simple example in a classical concept is to consider the situation in Figure 22. If you release the ball from point A, it cannot get over point B because it does not have enough to pass it. But in the quantum scale there exists a non-zero probability that a particle can be found on the other side of the barrier that is in point C. First by solving the wave function we can get information about the probability for the particle to be in a specific place. When this is plotted, we see that the wave function "penetrates" the potential barrier meaning that there is a non-zero probability. An example of this can be seen in Figure 23 where one can see four different wave functions with different energy eigenvalues. Two of these are in the area where the potential barrier has an impact. You can see that the wave function does not vanish when the linear potential barrier begins so there is a possibility to find the particle on the other side when you measure its position. This seems absurd if you have no knowledge of the quantum theory. How is it possible?

Quantum tunneling was first discovered in 1927 by Friedrich Hund when he was calculating the solutions for the double-well potential [22]. Later Max Born generalized the idea and concept into the whole quantum theory. To give some perspective one nanometer is 10^{-9} meters. The barrier thickness for tunneling usually is in the

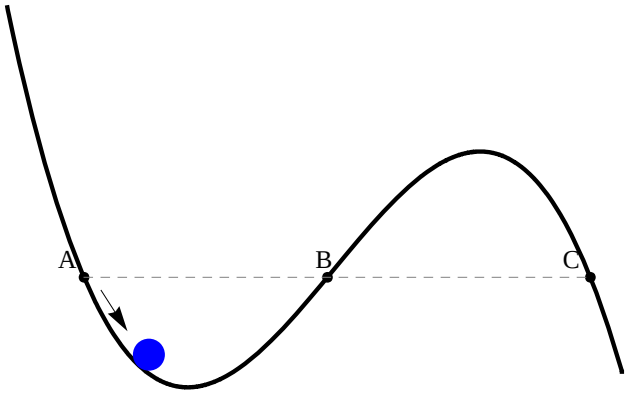

Figure 22: Classical example of a ball in a valley.

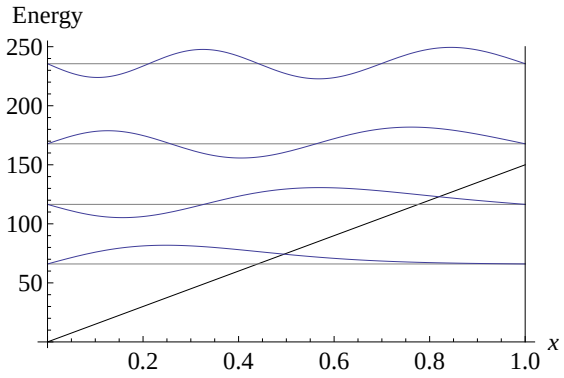

Figure 23: Linear potential barrier in a box. The potential is described by the black line. There are four different wave functions, which are the blue curves, with different energy eigenvalues. The two lowest ones can go through the barrier. The x-axis describes the position and the y-axis describes the energy.

range of less than 3 nanometers [42]. The tunneling probability for larger objects is very small. That is why you have never seen an elephant go through a wall. Tunneling is a key part for example in nuclear fission. Fission is the mechanism which powers our nuclear plants. In practise it means that one atomic nucleus splits into two smaller atomic nuclei and the reaction releases a vast amount of energy. Other applications that use the tunneling property include the tunnel diodes [43], which work very fast compared to normal diodes, and the scanning tunneling microscope [44], which can make 3-dimensional images of the atom structure of the surface of a metal. So not only being one the cornerstones in quantum theory, it is related to advanced study of modern technology and applications. It is therefore interesting to think about what is happening and how, and that question leads us to the philosophical side.

4.1.2 Different approaches

Because quantum physics is so bizarre, there exists also different philosophical ways to interpret it. There are many opinions about these and still there is no solution that would satisfy all physicists. Every interpretation has its own advantages and problems but of course they all give the same result in the end, even though some of them might have different amount of pre-assumptions. Since we can basically only measure the incomes and outcomes, and are not really able to look in a classical way what is happening during the tunneling, the ultimate conclusion of these different interpretations will have to wait. Also the mathematical formalism does not tell us

what is going on in the subatomic level. So we need to raise some metaphysical and ontological questions. Let us have a quick look into a couple of the most known theories.

The Copenhagen interpretation was mainly developed by Niels Bohr and Werner Heisenberg with the assistance of other physicists in 1920s.[45] This is considered to be the orthodox way to explain quantum mechanics and its phenomena. It is also the most widely taught theory but there are still different versions of it that slightly differ from each other. It is a non-deterministic theory which for instance says that it is irrelevant to ask where has the particle been before. It only matters after you measure it which gives a very high status for measuring. When you measure for example the particle's position, its wave function collapses according to the Copenhagen interpretation. Collapsing means that when it is measured, the wave function collapses into one random state of all the possible states. With the mathematical wave function we can only see the states that are more probable than others and then measuring "picks out" one them. The existence of the particle before measurement is an interesting question. We at least think we know that it exists but we do not know where. But only after the measurement it becomes certain and what happened before that does not matter anymore. Applied to the tunneling it proposes that because of the Heisenberg uncertainty principle there cannot be a precise position and momentum at the same time. The interpretation wipes out the problem of penetrating the barrier by stating that if we localize the particle, the energy momentum becomes irrelevant. So the particle does not anymore have energy and especially it does not need more energy to pass the barrier.[46] Therefore the problem is gone.

Hugh Everett formulated the many-worlds interpretation in 1965.[47] This formalism denies that the wave function could collapse. In fact it contains every possible alternative histories and futures which are all real. Every one of those histories and futures represents its own world and from this comes the name of the interpretation. Basically there is a very large or infinite number of different universes and we just happen to be in one the universes contained by a multiverse. The theory also denies access to the parallel universes which is due to quantum decoherence. It claims also that physical phenomena are always deterministic in the multiverse but in our universe they seem to be non-deterministic because we can only observe things happening here. How about the quantum tunneling? Of course it is easy to say that in some universe the particle can be found on the other side of the barrier but that does not tell the reason for it nor it does not tell what happens in the

actual tunneling.

There are also a number of more interpretations which we will not look into deeper. Some of them contain for instance hidden variables which was a quite popular theory in its time. It was John Bell who smashed the dreams from those theories by his inequalities that deny the hidden variables.[48] There exists also theories and interpretations not made by physicists but it is fairly easy to discard those because it is no in any way possible to make these kinds of assumptions without knowing the basic mathematical background.

4.1.3 Discussion

The question about tunneling and its meaning is quite tricky after all. The Copenhagen interpretation explains it in a way but it still leaves questions. The interpretation itself has also gotten a lot criticism of not being consistent all the time. Also the idea of the collapsing wave function is one the things that has been talked a lot. It is strange that in quantum scale there would be a wave-particle behavior but when we measure we have a distinct particle. Many-worlds theory on the other hand is also interesting even though it does not really say anything about tunneling. The theory also has the major downside that it is hard to show that the theory is correct by measuring it. It is also said that in tunneling the trace of the particle is singular and reappears again after the barrier.[49]

One could also always argue that does quantum tunneling really even exist? Could it just be a way to explain things that we do not really comprehend at all? Of course there is no way of denying the experiments where the particles have actually been found on the other side. But can we truly rely that our equations are correct? For example Newtonian mechanics was considered to be the absolute truth for hundreds of years until Einstein changed that. We also know for a fact that our equations in quantum physics and relativity are inadequate because they do not unite to a single theory in the form they are now. Denying tunneling is still too harsh because even though the quantum theory is not the theory of everything, it is still the most accurate physical theory that has been tested. The denial comes easily towards things you cannot see or understand. Quantum tunneling is just one of the unique phenomena that occur in our universe. Although some have proposed also an idea about high-jumping. In that concept the particle can borrow energy from self-interference so that it can go over the barrier [50].

It is a deep philosophical question to wonder why does the quantum mechanics work and in this case why does quantum tunneling occur. That is why we have

these different interpretations and theories because the mathematics itself does not explain the essence of it. On the other hand when you know the outcome result you want to have, it is in some sense easy to start to formulate a way to get there. Of course you will have to have substantial knowledge of the theory and mathematics to be able to do this. We might have to wait for a bigger theory before we can have more certainty to the answers. Although then we will probably end up asking new questions.

4.2 Tunneling time

One very interesting notion is the concept of tunneling time. This is in other words the time that the particle spends in the classically forbidden region. In 1932 MacColl discovered that tunneling probability is not the only thing to consider but it also takes time for the particle to penetrate the barrier.[51] There have been various attempts to define the right formalism, definition and operators for the tunneling time but still there is no consensus about the matter.[52] Thomas E. Hartman stated in 1962 that if the barrier is not too opaque, the tunneling time becomes independent of the barrier width.[53] This is called the Hartman effect. It also implies that if the barrier is large, the effective velocity of the particle can become arbitrarily large and even larger than the speed of light in some cases. These faster-than-light cases do not actually violate special relativity because this can only happen to virtual particles, and by that the information transfer velocity is less than the speed of light. A good question is to think about what is happening to the particle when it is crossing the barrier.

4.3 Path integrals and instantons

4.3.1 Introduction

The aim of the instanton solution is to present the transition probability that a particle tunnels through a potential barrier. This has been studied especially for the double well potential. In an instanton solution we try to find a solution corresponding to the classical system of motion but with a difference that it is done with an imaginary time. We substitute $t = -i\tau$ and consider the semi-classical limit where $\hbar \to 0$. In this approach we use the Feynman path integral theory. This theory does not use operators or the Schrödinger equation which opens a lot of different possibilities that the canonical theory of quantum mechanics does not have.

In this section we refer mainly to [8] and [54]. The basic idea of Feynman path integral is that it gives the amplitude for a particle with an initial state $|\psi_i\rangle$ at time $t = t_i$ to be in a final state $|\psi_f\rangle$ at time $t = t_f$ in the following form

$$\begin{aligned}\langle \text{final}, t_f \mid \text{initial}, t_i\rangle =& \langle \text{final}, t_f \mid e^{\frac{i}{\hbar}(t_f - t_i)\hat{H}(\hat{X},\hat{P})} \mid \text{initial}, t_i\rangle \\ =& \int_{\text{initial},t_i}^{\text{final},t_f} e^{\frac{i}{\hbar}\int (p\dot{q} - h(p,q))\, dt}\, dpdq\end{aligned} \tag{122}$$

where $\hat{X}$ is the position operator, $\hat{P}$ is the momentum operator, $\hat{H}(\hat{X}, \hat{P})$ is the Hamiltonian of the quantum theory and h(p,q) is the Hamiltonian of the classical theory. The calculation is done by summing over all the possible classical paths so that they satisfy also the boundary conditions.

We will first introduce some of the aspects of the basic path integral theory and then go to the actual tunneling problem. The starting point is the focus with the time evolution operator

$$\hat{U}(t_f, t_i) = e^{-\frac{i}{\hbar}(t_f - t_i)\hat{H}(\hat{X},\hat{P})}. \tag{123}$$

This means that in the case of no time dependence in the Hamiltonian $\hat{H}(\hat{X}, \hat{P})$ we can calculate the wave function $|\Psi(t)\rangle$ at any time t_b with the time evolution operator from any other time t_a by operating in the following way

$$|\Psi(t_b)\rangle = \hat{U}(t_b, t_a)|\Psi(t_a)\rangle. \tag{124}$$

The time evolution operator thus satisfies the Schrödinger equation

$$\hat{H}\hat{U}(t, t_a) = i\hbar\partial_t\hat{U}(t, t_a). \tag{125}$$

It is also a unitary operator

$$\hat{U}(t_b, t_a) = \hat{U}^{-1}(t_a, t_b) \tag{126}$$

and it satisfies the composition law for time translations

$$\hat{U}(t_b, t_a) = \hat{U}(t_b, t')\hat{U}(t_a, t'). \tag{127}$$

The point in here is to get the time evolution amplitudes that are given by the matrix elements of the time evolution operator in the basis states that are localized.

With these we get the equation (122) in the form

$$(\psi_f t_f \mid \psi_i t_i) = \langle \psi_f \mid \hat{U}(t_f, t_i) \mid \psi_i \rangle \tag{128}$$

where we have obviously assumed that $t_f > t_i$. The notation $(\psi_f t_f \mid \psi_i t_i)$ is also called the propagator of the system. The propagator also satisfies the Schrödinger equation because of the properties of the time evolution operator

$$\hat{H}(\psi t \mid \psi_i t_i) = i\hbar\partial_t(\psi t \mid \psi_i t_i) \tag{129}$$

and if the Hamiltonian has no time dependence it can be calculated by

$$(\psi_f t_f \mid \psi_i t_i) = \langle \psi_f \mid e^{-\frac{i}{\hbar}(t_f - t_i)\hat{H}} \mid \psi_i \rangle. \tag{130}$$

Here by showing all these we end up having the equation (122) from which we started the whole thing.

We are especially interested in the case where 1-dimensional quantum tunneling can occur through a barrier. In classical physics this is of course forbidden because a particle cannot go to a region which has a larger potential energy than the total energy of the particle. This would classically require a negative kinetic energy which is not possible as we know it. We can observe this from the equation for the total energy E

$$E = T + V = \frac{1}{2}m\dot{q}^2 + V(q), \tag{131}$$

where q is the particle position and the derivative $\dot{q}$ is the velocity of the particle. Here it can be seen that if it were that $E < V$, it would require that $T < 0$. Meaning that the velocity to the power of two would be negative which is obviously impossible when we are dealing with physics and real numbers. So something has to be done. The imaginary time, which we spoke of earlier, is the key element here. When the time variable is imaginary, then the momentum becomes real and the motion becomes imaginary.

If the particle starts from $x = x_i$ and ends up in $x = x_f$ at the time T, we get the tunneling probability as a square of the absolute value of the Feynman propagator $D_F(x_f; x_i, T, 0)$. It can be formally determined as a sum over the classical paths

$$D_F \sim \int [\mathcal{D}(x)] e^{\frac{i}{\hbar}S(x)}. \tag{132}$$

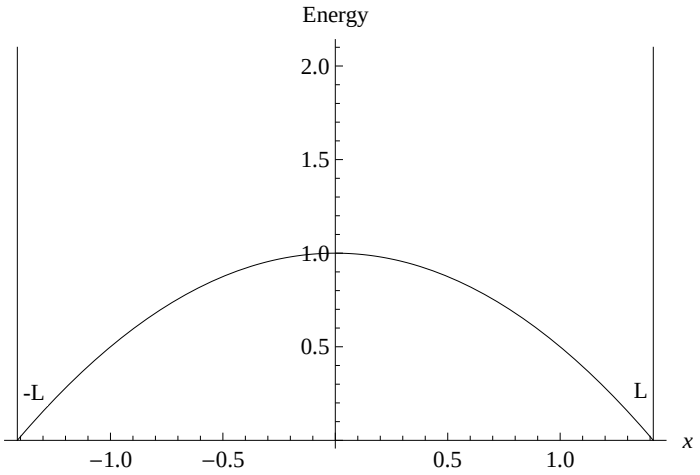

Figure 24: Example of the potential (133). $E_0 = 1$, $k = 1$ and $L = \sqrt{2}$.

We have discussed the different approaches to the mathematical formalism of the quantum theory. The earliest two formalisms are the matrix mechanics of Heisenberg and later on the wave function theory of Schrödinger. A few years later Paul Dirac showed these to be equivalent. In this work up until this point we have used in our calculations the Schrödinger equation. A quite simple calculation will demonstrate what is the connection between the Schrödinger equation and Feynman theory of the path integrals in quantum mechanics.[55]

Further reading and a much more mathematical approach to the path integrals can be found in the reference [56]. It is more focused in the Yang-Mills theory and by so it goes way deeper into this subject. The instanton solutions are shown in four dimensions. It deals with how the instantons are a part of different studies in physics going all the way from supersymmetry to the Higgs fields. Next we will go to the actual tunneling problem of the inverted oscillator potential in an infinite well.

4.3.2 Infinite well with an inverted oscillator potential

We will explore the possibilities of the path integral method to investigate the tunneling. Our potential is chosen to be the inverted oscillator in an infinite well which is the potential investigated in Chapter 3. We are especially interested in how this resembles the normal double-well potential case which is the classic example of this procedure. We are to find the instanton solution for our chosen potential. The

explicit potential inside the well is

$$V(x) = E_0 - \frac{1}{2}kx^2, \tag{133}$$

where we have taken in the energy coefficient E_0 to avoid negative energies which are natural in this case without the coefficient. E_0 is just for scaling and it also tells us what is the height of the potential barrier in its center position. In the potential we have two minima at

$$x_{min} \equiv \pm L \tag{134}$$

and as you can see these parameters marked in Figure 24 the minima is where the potential hits the wall on the sides. The parameter L for length is then of course with the other parameters

$$L = \sqrt{\frac{2E_0}{k}}. \tag{135}$$

In search of the instanton solution we begin with the equation of motion and at this point we are still in real time

$$\ddot{x}(t) = -V'(x(t)) \tag{136}$$

where we have marked the derivatives in the following manner

$$\begin{aligned} \ddot{x} &= \frac{d^2x}{dt^2} \\ V'(x) &= \frac{dV(x)}{dx}. \end{aligned}$$

Now we make the replacement and move from real into imaginary time by inserting

$$\tau = -it \tag{137}$$

We get the equation of motion in imaginary time

$$x''(\tau) = V'(x(\tau)) \tag{138}$$

where the derivatives are

$$\begin{aligned} x''(\tau) &= \frac{d^2x}{d\tau^2} \\ V'(x(\tau)) &= \frac{d^2V}{d\tau}. \end{aligned}$$

This is now the equation of motion for the reverse of the potential (133) which means that the potential is upside down as can be seen when compared to (136). Let us start working on this and we keep in mind that the goal is to solve $x(\tau)$. First we multiply (138) by $x' = dx/d\tau$

$$\begin{array}{lll} \text{Left side:} & x'(\tau)x''(\tau) & = \frac{1}{2}\frac{d}{d\tau}x'(\tau)^2 \\ \text{Right side:} & x'(\tau)\frac{dV(x(\tau))}{dx(\tau)} & = \frac{dV}{dx}\frac{dx}{d\tau} = \frac{dV(x(\tau))}{d\tau} \end{array}$$

We end up having

$$\frac{1}{2}\frac{d}{d\tau}x'(\tau)^2 - \frac{d}{d\tau}V(x(\tau)) = 0. \tag{139}$$

We will integrate this on both sides with respect to τ. This gives us directly due to the function being continuous

$$\frac{1}{2}x'(\tau)^2 - V(x(\tau)) = C, \tag{140}$$

where C is the integration constant. To emphasize even more that we are dealing with the reversed potential we will write (140) in the form

$$\frac{1}{2}x'(\tau)^2 + [-V(x(\tau))] = C. \tag{141}$$

Now that we look at it we actually notice that this is the energy conservation law if τ is interpreted as the physical time. It is for the motion in the potential $-V(x)$ and by that we can make the assumption that the constant C is actually the total energy E. You can compare this to the equation (131) on page 63. We can now in relief make the replacement

$$C \equiv E$$

to the equation (141) and integrate it once more. With this short calculation

$$\begin{aligned} \frac{dx}{d\tau} &= \pm\sqrt{2(E+V(x))} \\ \int_{\tau_0}^{\tau} d\tau &= \pm\frac{1}{\sqrt{2}}\int_{x(\tau_0)}^{x(\tau)} \frac{dx}{\sqrt{E+V(x)}} \end{aligned}$$

it yields that

$$\tau - \tau_0 = \pm\frac{1}{\sqrt{2}}\int_{x(\tau_0)}^{x(\tau)} \frac{dx}{\sqrt{E+V(x)}}. \tag{142}$$

It is good to notice that this is valid for a general potential $V(x)$. So here we need our actual potential (133). By looking at the potential figure 25 we will see that if our particle starts at rest and goes along with $\tau \to -\infty$, we must have $E = 0$. Now we see why we inserted the parameter E_0 into our potential. Otherwise it would have given us a negative root. Having these we can integrate (142) from 0 to x. For $-L < x < L$ we get

$$\begin{aligned} \tau - \tau_0 &= \pm\frac{1}{\sqrt{2}}\int_0^x \frac{dz}{\sqrt{E_0 - \frac{1}{2}kz^2}} \\ &= \pm\frac{1}{2\sqrt{k}}\int_0^x \frac{dz}{\sqrt{\frac{2E_0}{k} - z^2}} \\ &= \pm\frac{1}{2\sqrt{k}}\arcsin\left(\sqrt{\frac{k}{2E_0}}x\right). \end{aligned} \tag{143}$$

Now we have finally reached to the point of having the instanton solution for the inverted oscillator and it is

$$x_\pm(\tau) = \pm\sqrt{\frac{2E_0}{k}}\sin\left[2\sqrt{k}(\tau - \tau_0)\right], \tag{144}$$

where we have used the trigonometric formula

$$\sin(\pm x) = \pm\sin(x).$$

The solution (143) can be seen in Figure 26. It shows that the solutions are at zero when the potential is at the highest and they go to infinity on the edges of the well. The instanton solution (144) is in Figure 27 which shows a nice symmetry. The instanton solution is also called the kink and anti-kink solution.

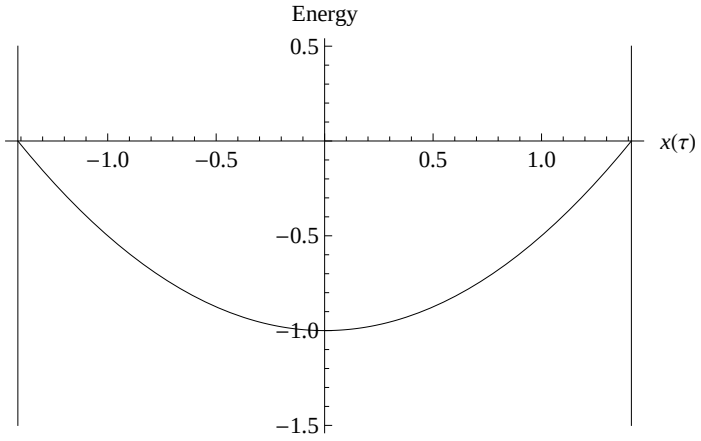

Figure 25: Example of the reversed potential (133). $E_0 = 1$, $k = 1$ and $L = \sqrt{2}$.

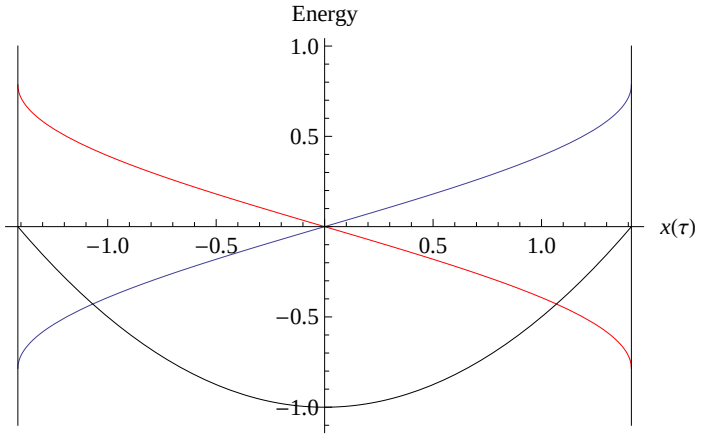

Figure 26: The solutions for $\tau - \tau_0$ in (143). The blue line is the positive solution and the red line is the negative solution. $E_0 = 1$, $k = 1$ and $L = \sqrt{2}$.

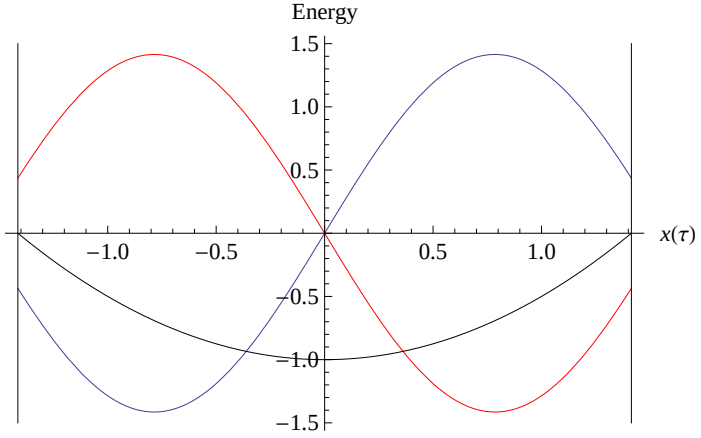

Figure 27: The instanton solutions (144). The blue line is the positive solution and the red line is the negative solution. $E_0 = 1$, $k = 1$ and $L = \sqrt{2}$.

We can go further and calculate the Euclidean action A for this system

$$\begin{aligned} A &= \int_{-\infty}^{\infty} \left[\frac{x_{\pm}'^2}{2} + V(x_{\pm}(\tau)) \right] d\tau \\ &= \int_{-\infty}^{\infty} \left(x_{\pm}'^2 - E \right) d\tau \\ &= -EL + \int_{-a}^{a} \sqrt{2(E + V(x))} dx \end{aligned}$$

It comes handy when we insert $E = 0$, plug in the potential (133) and the condition (135)

$$\begin{aligned} A &= \int_{-a}^{a} \sqrt{2E_0 - kx^2} dx \\ &= \int_{-\sqrt{\frac{2E_0}{k}}}^{\sqrt{\frac{2E_0}{k}}} \sqrt{2E_0 - kx^2} dx \\ &= \frac{E_0}{\sqrt{k}} \pi. \end{aligned} \tag{145}$$

When we start comparing these to the solutions of the symmetric double-well potential, we will see lots of similarities. We will first give the results for the double-well potential and they are made according to [8]. The potential $V_{\text{double}}(x)$ is of the form

$$V_{\text{double}}(x) = \frac{\omega^2}{8a^2}(x - a)^2(x + a)^2, \tag{146}$$

where minimas are located at $x = \pm a$ and the coupling constant g is

$$g = \frac{\omega^2}{2a^2}. \tag{147}$$

Now we can follow the procedure introduced above and by integrating (142) and setting $E = 0$ we get for $-a < x < a$ that

$$\tau - \tau_0 = \pm \frac{2}{\omega} \operatorname{arctanh} \left(\frac{x}{a} \right), \tag{148}$$

which is shown in Figure 28. The instanton solution for the barrier crossing in the

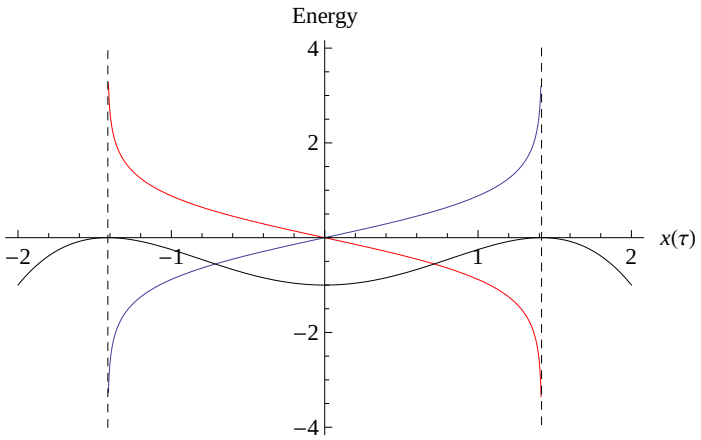

Figure 28: The solutions for $\tau - \tau_0$ in (148). The blue line is the positive solution and the red line is the negative solution. $a = \sqrt{2}$, $\omega = 2$.

symmetric double-well potential is

$$x_{\pm}(\tau) = \pm a \tanh\left[\frac{2}{\omega}(\tau - \tau_0)\right], \tag{149}$$

which is shown in Figure 29. The Euclidean action for this system is

$$A_{\text{double}} = \frac{\omega^3}{3g}. \tag{150}$$

Now we have the required formula for the double-well system.

We can see that the two cases are basically quite similar. They both have their solutions at zero when the potential is at its maximum. In the $\tau - \tau_0$ solution both have infinities on the edges, and the actual instanton solution also has a resemblance.

4.3.3 Summary

We have represented the basics of the path integral theory and found a way to have an instanton solution for our quantum system, the inverted harmonic oscillator in an infinite well. The basic example is the instanton solution for double-well potential which is also our comparison point. This is interesting also because of the resemblance of our quantum system and the double-well potential. The two of them share many same qualities as we have seen before in previous chapters.

The important notion is that we can do our solution similarly with the double-well potential. The solution is in the form of *sin*-function as for the double-well is a *tanh*-function. These may seem distant but qualitatively they are quite alike.

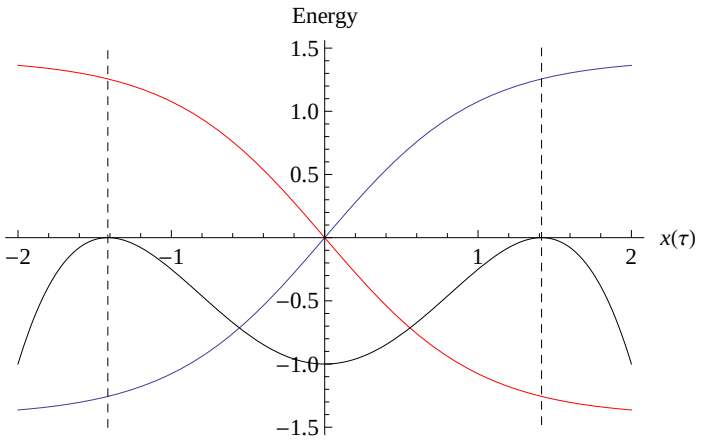

Figure 29: The instanton solutions (149). The blue line is the positive solution and the red line is the negative solution. $a = \sqrt{2}$, $\omega = 2$.

We have to remember that we are not dealing with $x \in \mathbb{R}$ because of our boundary conditions. This will isolate the situation so that in our area of research the results seem to be quite similar. Altogether it is worthy to notice that we have a solution and it shows up to be consistent with the double-well potential solution.

Conclusions

We have studied the properties of two quantum potentials, 1-dimensional linear potential in an infinite well and 1-dimensional inverted oscillator in an infinite well. The motivation for our study comes from experimental background where we have a 3-dimensional cylinder with magnetic fields that can be adjusted. The magnetic fields can be simplified as our potentials if we look at them in a 1-dimensional situation. For these potentials we have the solutions for energy eigenvalues and eigenfunctions by using different numerical methods.

The essential part in Chapter 1 is that it deals with the fact that there are different ways to approach the mathematical formalism of quantum mechanics. All of them share some similar properties but there are properties that can easily be gained from a specific formalism. This is why we use the desired formalism based on the properties that we are currently studying. In Chapters 2 and 3 we are using the traditional Schrödinger equation because it gives us the solutions for the energy eigenstates. In Chapter 4 on the other hand we represent the path integral theory created by Richard Feynman. This gives us access to the instanton solutions which is used studying the tunneling properties. Our work serves as an example of how to use different methods for different aspects.

The actual study begins with the linear potential in an infinite well. This is an enclosed system which gives us boundary conditions. In this particular situation we want to use and compare two different boundary conditions. First we have the normal boundary conditions (44) where the wave function goes to zero on the edges of the well. The derivative boundary conditions (45) make the derivative of the wave function go to zero on the edges of the well. The motivation for the derivative conditions comes from the experimental background. The derivative boundary is a way to get the spin wave situation which is the case in the experiments. So now by using a numerical method we get the solutions for both of the conditions as a sum of Airy function that are dependent of the potential parameter k and the length of the well L. The results are quite as expected. They start to resemble the particle in a box when the potential parameter is small. In the impact area of the potential we have the possibility to be in the classically forbidden area. We also compare the results to the Flügge solution where we have an infinite wall only on the left side. We have specific approximation formula for the energies in the Flügge situation which we use to compare our results. When the potential slope is large our results are very similar to the Flügge solution which is a bit surprising. Figure 15 is a highlight of the comparison between the two solutions. We see that the results start to differ

immediately when we are no longer on the impact area of our linear potential.

The inverted oscillator in an infinite well is also equipped with boundary conditions. In this case we only use the normal boundary (113) where the wave function goes to zero on the edges of the well. The actual oscillator is symmetric and confined from $x \in [-L, L]$ which means that the size of the well is $2L$. After we have done the substitutions (105), (106) for the variables we are free of the potential parameter k. Our system is now only dependent on the length of the well L. This means that making the well wider will also make the potential slope grow. It is convenient to make this substitution because it reduces the burden of the numerical data and even a bit surprisingly it works. Again with the solutions we see that they resemble the particle in a box if we have a small potential slope. We have shown three different situations - small, medium and large. The medium case shows that after the potential impact the resemblance of the particle in a box returns. But the large box is something different. There the situation reminds us of the double-well potential. We have a very strong pairing between the even and odd energy eigenstates. It is notable that the pairing continues even after we are above the actual potential curve. It would also be interesting to do the solutions for the asymmetric inverted oscillator. It would make the calculations even longer and it might be a case to think of a different numerical method.

It is a good time to think what are the equal properties of our the potentials that we have investigated. The key thing is that they both resemble the solution of the particle in a box when the potential curve is small enough. This can be seen from figures and from the energy eigenvalue ratios that have been compared. They both have the possibilities for the particle being in the classically forbidden area. The solutions are given by special functions. With the linear potential we have the Airy functions and with the inverted oscillator we have the parabolic cylinder functions. The cases use numerical methods that were different. With the linear potential the numerics did not require that much of computer power. All in all it was quite simple and handy. The inverted oscillator has more complex functions and the method for the linear potential did not work. We have used a polynomial solution by cutting the series to a specific point and solving the zero points for the equations. It took quite a lot of computer power and we had to adjust the polynomial factor N according to each case to make the solutions as good as they can be. A key difference is that when the potential is large the linear potential starts to resemble the Flügge solution until the potential impact is gone, and the inverted oscillator has the pairing property which reminds of the double-well potential.

We have also discussed about the tunneling in quantum mechanics. The first approaches it has had starting from the beginning of the 20th century and going from that to a specific way using the path integral theory to examine the tunneling properties of a quantum system. We have shown that we can solve the instanton solution for the inverted oscillator in an infinite well. The method to do this is similar to instanton solution of the double-well potential. When we are dealing with the confined quantum system, the two cases are qualitatively quite similar in the region of our perspective.

All in all our goals and achievements have been accomplished. We have all the solutions we went for and we also gained some important nontrivial results. It is worthy to notice that our actual quantum potentials might seem trivial but after all they require quite a lot of work. The most significant things are the accuracy with the Flügge solution, the strong pairing of the even and odd solutions with the inverted oscillator, having only one parameter in the solutions with the inverted oscillator, and finally having the an instanton solution for the inverted oscillator.

Acknowledgements

This work is a tribute for my newborn daughter, Ilona. Thank you Maarit for the endless support and love. My heart also belongs to you Atte and Inka.

I would also like to say a thanks to Roope Uola for lending me more efficient computer power for some of the calculations, and giving good advices and support.

References

[1] M. Born, "Max Karl Ernst Ludwig Planck. 1858–1947", Obituary Notices of Fellows of the Royal Society **6** (17): 161 (1948)

[2] E. Schrödinger, "An Undulatory Theory of the Mechanics of Atoms and Molecules", Phys. Rev. **28**, 1049 (1926)

[3] W. Heisenberg, "Über quantentheoretische Umdeutung kinematischer und mechanischer Beziehungen", Z. Phys. **33**, 879 (1925)

[4] I.J.R. Aitchison, D.A. MacManus, T.M. Snyder, "Understanding Heisenberg's "magical" paper of July 1925: A new look at the calculational details", Am. J. Phys. **72**, 1370.6 (2004)

[5] P. Dirac, "The Principles of Quantum Mechanics", Oxford: Oxford University Press (1930)

[6] K. Gottfried, "P.A.M. Dirac and the Discovery of Quantum Mechanics", arXiv:quant-ph/0302041 (2003)

[7] R.P. Feynman, "Space-Time Approach to Non-Relativistic Quantum Mechanics", Rev. Mod. Phys. **20**, 367 (1948)

[8] H. Kleinert, "Path Integrals in Quantum Mechanics, Statistics, Polymer Physics, and Financial Markets", 4th edition, Singapore: World Scientific Publishing Co. (2006)

[9] R. Dum, A. Sanpera, K.-A. Suominen, M. Brewczyk, M. Kus, K. Rzazewski, and M. Lewenstein, "Wave Packet Dynamics with Bose-Einstein Condensates", Phys. Rev. Lett. **80**, 3899 (1998)

[10] O. Vainio, J. Ahokas, S. Novotny, S. Sheludyakov, D. Zvezdov, K.-A. Suominen, and S. Vasiliev, "Guiding and Trapping of Electron Spin Waves in Atomic Hydrogen Gas", Phys. Rev. Lett. **108**, 185304 (2012)

[11] O. Vainio, J. Ahokas, J. Järvinen, L. Lehtonen, S. Novotny, S. Sheludiakov, K.-A. Suominen, S. Vasiliev, D. Zvezdov, V. V. Khmelenko, and D. M. Lee, "Bose-Einstein Condensation of Magnons in Atomic Hydrogen Gas", Phys. Rev. Lett. **114**, 125304 (2015)

[12] S. Flügge, "Practical Quantum Mechanics", 2nd Edition, Berlin: Spinger-Verlag (1994)

[13] G. J. Milburn, J. Corney, E. M. Wright, and D. F. Walls, "Quantum dynamics of an atomic Bose-Einstein condensate in a double-well potential", Phys. Rev. A **55**, 4318 (1997)

[14] S.N. Bose, "Plancks Gesetz und Lichtquantenhypothese", Z. Phys. **26**, 178–181 (1924)

[15] D.D. Stancil and A. Prabhakar, "Spin Waves: Theory and applications", New York: Springer (2009)

[16] L. de Broglie, "Nobel Lecture: The Wave Nature of the Electron", Physics 1922-1941, Amsterdam: Elsevier Publishing Company (1926)

[17] B. R. Johnson, J. S. Denker, N. Bigelow, L. P. Lévy, J. H. Freed, and D. M. Lee, "Observation of Nuclear Spin Waves in Spin-Polarized Atomic Hydrogen Gas", Phys. Rev. Lett. **52**, 1508 (1984)

[18] D.M. Lee, "Spin Waves in Spin Polarized Hydrogen", Jpn. J. Appl. Phys. **26**, 1841 (1987)

[19] N. P. Bigelow, J. H. Freed, and D. M. Lee, "Nuclear-spin waves in polarized atomic hydrogen gas: Temperature and density dependence in the hydrodynamic and Knudsen regimes", Phys. Rev. Lett. **63**, 1609 (1989)

[20] C. Lhuillier and F. Laloë, "Transport properties in a spin polarized gas, I", J. Phys. France **43**, 197 (1982)

[21] C. Lhuillier and F. Laloë, "Transport properties in a spin polarized gas, II", J. Phys. France **43**, 225 (1982)

[22] F. Hund, "Zur Deutung der Molekülspektren", Z. Phys. **40**, 742-764 (1927)

[23] M. Abramowitz, I.A. Stegun, eds., "Handbook of Mathematical Functions with Formulas, Graphs, and Mathematical Tables", New York: Dover (1965)

[24] G.B. Airy, "On the Intensify of Light in the neighbourhood of a Caustic", Transactions of the Cambridge Philosophical Society (University Press) **6**: 379–402 (1838)

[25] G.B. Airy, "The Autobiography of Sir George Biddell Airy", Cambridge: Cambridge University Press (1896)

[26] J. Dutka, "On the early history of Bessel functions", Archive for History of Exact Sciences, Volume 49, Issue 2, 105 (1995)

[27] N. Zettili, "Quantum Mechanics: Concepts and Applications", 2nd edition, New Jersey: Wiley (2009)

[28] H. Ruskeepää, "Mathematica Navigator: Mathematics, Statistics and Graphics", 3rd edition, Waltham: Academic Press (2009)

[29] P. Weiss, "Prof. Dr. Heinrich Friedr. Weber, 1843–1912", Schweizerische Naturf. Ges. Verh. **95**, 44 (1912)

[30] H.F. Weber, "Über die Integration der partiellen Differentialgleichung $u''(x) + u''(y) + k^2u = 0$", Math. Ann. **1**, 1 (1869)

[31] E.T. Bell, "Men of Mathematics", New York: Simon and Schuster (1986)

[32] F.C. Rotbart, "Quantum symmetrical quadratic potential in a box", J. Phys. A **11**, 2363 (1978)

[33] V.C. Aguilera-Navarro, E. Ley Koo, and A.H. Zimerman, "Perturbative, asymptotic and Padé-approximant solutions for harmonic and inverted oscillators in a box", J. Phys. A **13**, 3585 (1980)

[34] F.C Auluck and D.S. Kothari, "Energy-levels of an artificially bounded linear oscillator", Science and Culture **7**, 370 (1940)

[35] F.C. Auluck, "Energy levels of an artificially bounded linear oscillator", Proc. Nat. Inst. India **7**, 133 (1941)

[36] F.C. Auluck and D.S. Kothari, "The quantum mechanics of a bounded linear harmonic oscillator", Proc. Camb. Phil. Soc. **41**, 175 (1945)

[37] J.S Baijal and K.K. Singh, "The energy-levels and transition probabilities for a bounded linear harmonic oscillator", Prog. Theor. Phys. **14**, 214 (1955)

[38] P. Dean, "The constrained quantum mechanical harmonic oscillator", Proc. Camb. Phil. Soc. **62**, 277 (1966)

[39] R. Vawter, "Energy eigenvalues of a bounded centrally located harmonic oscillator" J. Math. Phys. **14**, 1864 (1973)

[40] A. Consortini and B.R. Frieden, "Quantum-mechanical solution for the simple harmonic oscillator in a box", Nuovo Cim. B **35**, 153 (1976)

[41] V.C. Aguilera-Navarro, H. Iwamoto, E. Ley Koo, and A.H. Zimerman, "Quantum-mechanical solution of the double oscillator in a box", Nuovo Cim. B **62**, 91 (1981)

[42] R.G. Lerner and G.L. Trigg, "Encyclopedia of Physics", 3rd edition, New York: Wiley (2005)

[43] R. Tsu and L. Esaki, "Tunneling in a finite superlattice", Appl. Phys. Lett. **22**, 562 (1973)

[44] E. Ruska, G. Binnig, and H. Rohrer, "Nobel Lecture: Scanning Tunneling Microscopy – From Birth to Adolescence", Physics 1981-1990, Singapore: World Scientific Publishing Co. (1993)

[45] D. Howard, "'Who Invented the 'Copenhagen Interpretation?' A Study in Mythology", Philos. Sci. **71**, 669 (2004)

[46] G. Bacciagaluppi and M. Dickson, "Dynamics for Modal Interpretations", Found. Phys. **29**, 1165 (1999)

[47] B. DeWitt and N. Graham, "The Many-Worlds Interpretation of Quantum Mechanics", Princeton University Press (1973)

[48] J. Bell, "On the Einstein Podolsky Rosen Paradox", Phys. **1**, 195 (1964)

[49] M. Kermanshahi, "Universal Theory: A Model for the Theory of Everything", Boca Raton: Universal Publishers (2007)

[50] W. Guowen, "Realistic solution to the tunneling time problem", arXiv:0706.3510v1 [quant-ph] (2007)

[51] L.A. MacColl, "Note on the Transmission and Reflection of Wave Packets by Potential Barriers", Phys. Rev. **40**, 621 (1932)

[52] S. Bandopadhyay and A.M. Jayannavar, "Hartman effect and nonlocality in quantum networks", Phys. Lett. A **335**, 266 (2005)

[53] T.E. Hartman, "Tunneling of a wave packet", J. Appl. Phys. **33**, 3427 (1962)

[54] M. Razavy, "Quantum Theory of Tunneling", Singapore: World Scientific Publishing Co. (2003)

[55] J.H. Field, "Derivation of the Schrödinger equation from the Hamilton-Jacobi equation in Feynman's path integral formulation of quantum mechanics", Eur. J. Phys. **32**, 63 (2011)

[56] S. Vandoren and P. van Nieuwenhuizen, "Lectures on instantons", arXiv:0802.1862 [hep-th] (2008)

Appendix

In order to give a little more input we present the Mathematica commands and methods used in section 2. This will also work as a short guide for using Mathematica for it is a powerful program and gives a diverse range of different tools. We assume that the basics of Mathematica are familiar. A good reference for further usage is found in Mathematica Navigator: Mathematics, Statistics and Graphics by H. Ruskeepää.

In Appendix A we show the case of the linear potential in an infinite well with the normal boundary conditions. In Appendix B we show the case of the linear potential in an infinite well.

Appendix A

First of all the boundary conditions 44

```
ξ0[k_,En_] := -k^(-2/3)*En
ξL[k_,L_,En_] := k^(-2/3)(L*k-En)
```

Then we have the equation satisfying the boundary conditions. This corresponds to the equation (53) at page 18

```
g[k_,L_,En_] := AiryAi[-k^(-2/3)*En]*AiryBi[k^(-2/3)*(L*k - En)]
- AiryAi[k^(-2/3)*(L*k - En)]*AiryBi[-k^(-2/3)*En]
```

This is the equation (55) that we get from the boundary conditions (50). We will give it a name `B`

```
B[k_,En_] := -AiryAi[ξ0[k,En]]/AiryBi[ξ0[k,En]]
```

The wave function solution (54) is

```
Ψn[x_,k_,En_,A_] := A*AiryAi[k^(-2/3)(x*k - En)] +
B[k,En]*A*AiryBi[k^(-2/3)(x*k - En)]
```

After defining these we start to work with the numerics. First we plot the function `g[k,L,En]` with the desired values of the potential parameter `k` and the box length `L`. From the plotted figure we are interested in the values `En` that give the roots of the function `g[k,L,En]`. The actual values are easily accessible with the command `FindRoot`. With `FindRoot` you give an initial value and then the program searches the nearest root numerically using an algorithm based on Newton methods. If you give two initial values, the program uses an algorithm based on the secant method.

When we have the energy eigenvalues `En`, we need the coefficient `A`. This is done by normalizing the wave function. We just simply integrate the square of the absolute value of the wave function and then we can plot it. We will show one

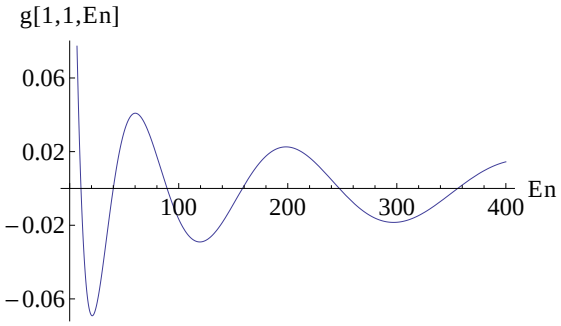

Figure 30: Function `g[k,L,En]` where $k = 1$ and $L = 1$.

demonstration on how this works in practice with these commands and what is the output. The same procedure works for the derivative boundary so we will not show it explicitly.

Example 1. Let $k = 1$ and $L = 1$. Now let us solve the corresponding energy values.

```
Plot[g[1,1,En],{En,0,400}]
```

The output for this can be seen in Figure 30. From this we check the points that we go hunting with `FindRoot`. We get for the first four values

```
FindRoot[g[1,1,En], {En, 10}]
En -> 10.3685
FindRoot[g[1,1,En], {En, 40}]
En -> 39.9787
FindRoot[g[1,1,En], {En, 90}]
En -> 89.3266
FindRoot[g[1,1,En], {En, 160}]
En -> 158.414
```

It is extremely convenient that we can check that these match to Figure 30. Now we need to normalize the wave function. The integral boundaries come from the choice of the box and so we get that

```
Integrate[Abs[Ψn[x,1,10.3685,A]]^2,{x,0,1}]
0.203809 (Im[A]^2 + Re[A]^2)
```

By the assumption that `A` $\in \mathbb{R}$ we get `A` by taking a square root of the reciprocal number of the result `0.203809`. Now we can plot the first energy eigenfunction.

```
Plot[Ψn[x,1,10.3685,1/√0.203809],{x,0,1}]
```

We can see the result in Figure 31.

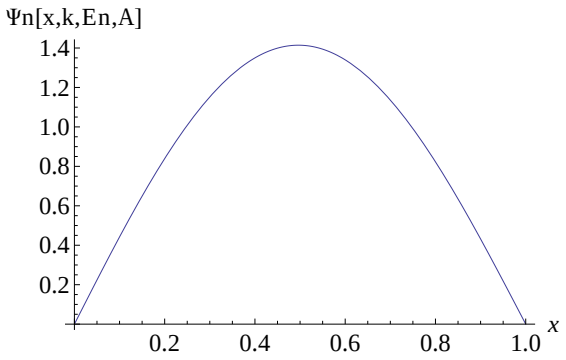

Figure 31: The first energy eigenfunction `Ψ[x,k,En,A]` where $k = 1$ and $L = 1$.

Appendix B

First we need to define the recursion (111)

```
c[a_,n_]:=c[a,n]=a*c[a,n-2]-((n-2)*(n-3)*c[a,n-4])/4
c[a,0]=c[a,1]=1
c[a,-2]=c[a,-1]=0
```

and then we can set the the wave functions. The even solution (109) is

`y1[a_,n_,t_,N_]:=1+Sum[(t^2n/(2n)!)*c[a,2n],{n,1,N}]`

and the odd solution 110 is

`y2[a_,n_,t_,N_]:=t+Sum[(t^2n+1/(2n+1)!)*c[a,2n+1],{n,1,N}]`.

Now we can start to solve the energy eigenvalues for the above functions `y1` and `y2` using `NSolve`. For this purpose we need to specify the polynomial factor N we need to use.The smaller N we use, the less eigenvalues we get. From the output we sort out the real solutions and discard the imaginary solutions by using `Reals`. After this we normalize the wave function and then we are ready to plot it.

We will once again show one example how to do this. It works in the same way for even and odd solutions.

Example 2. Let $L = \frac{\sqrt{2}}{4}$. Now let us use the `NSolve` for the energy eigenvalues. In this case we choose $N = 19$.

```
a /.  NSolve[y1[a, n, Sqrt[2]/4, 19] == 0, a, Reals]
a->{-1596.38, -967.211, -493.47, -177.643, -19.7351}
```

These are our energy eigenvalues. We plot the first eigenfunction after we have done the normalizing.

```
Plot[(0.3535735288567412‘)^-1/2*y1[a, n, t, 19] /.  a ->
-19.73512456489016‘,{t, -(Sqrt[2]/4), Sqrt[2]/4}]
```

The result is in Figure 32.

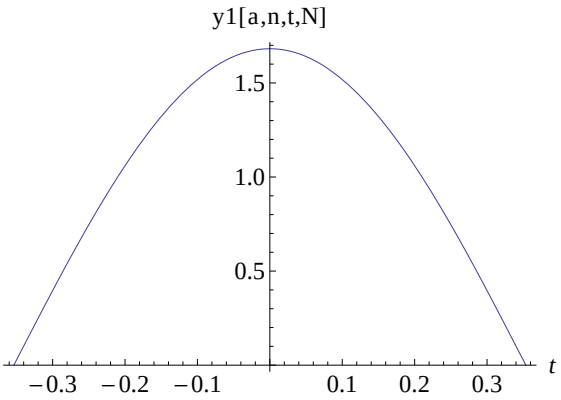

Figure 32: The first energy eigenfunction `y1[a,n,t,N]` where $L = \frac{\sqrt{2}}{4}$ and $N = 19$.